Biomass Conversion and Biorefinery
https://doi.org/10.1007/s13399-023-04098-9

ORIGINAL ARTICLE

Functional surface homogenization of nanobiochar with cation exchanger for improved removal performance of methylene blue and lead pollutants

Safe ELdeen M. E. Mahmoud[1,2] · David Ursueguia[2] · Mohamed E. Mahmoud[3] · Tarek M. Abel-Fattah[4] · Eva Díaz[2]

Received: 21 December 2022 / Revised: 14 March 2023 / Accepted: 16 March 2023

Abstract
Biochar materials are good examples of sustainable adsorbents with appreciable recent interests and applications in water treatment. The disadvantage of using unmodified pristine biochars in water treatment is mainly related to the inhomogeneous distribution of various surface functional groups. Therefore, the current study is designed to functionalize and homogenize the surface of a selected nanobiochar with a cation exchanger using hydrothermal and solvothermal microwave irradiation. The adsorption behavior of immobilized Amberlite cation exchanger onto Cynara scolymus nanobiochar (ACE@CSNB) was compared versus the pristine Cynara scolymus nanobiochar (CSNB). ACE@CSNB was categorized as a typical mesoporous material (mean pore size = 2.238 nm) and the FT-IR spectra confirmed surface modification via two characteristic peaks at 1140–1250 cm^{-1} and 1030–1070 cm^{-1} for R-SO_3^- with S = O. The TPD–MS analysis of CSNB and ACE@CSNB referred to the presence of carboxyl, lactonic, and acid anhydride groups as well as phenolic moieties. The adsorption behavior of methylene blue dye and lead ions by ACE@CSNB was found much higher than those concluded by CSNB providing maximum adsorptive capacity values owing to the played clear role by Amberlite cation exchanger. Moreover, ACE@CSNB was efficiently regenerated and confirmed MB and $Pb^{(II)}$ removal with 92.26% and 1000 µmol g^{-1}, respectively Finally, the removal efficiency values from three water matrices by ACE@CSNB biochar were characterized as 91.74–98.19% and 96.27–99.14% for $Pb^{(II)}$ and MB, respectively to refer to the validity and applicability of the investigated ACE@CSNB biochar for treatment of these two pollutants from real water samples with excellent efficiency.

Keywords Pristine and modified nanobiochars · Amberlite cation exchanger IR-120 (Na) · Adsorption behavior · Methylene blue and lead pollutants

1 Introduction

Application in water remediation of biochars as example of sustainable materials has been a hot topic in recent years owing to their excellent sustainability and low-cost for mass production [1]. Biochars are characterized as stable carbonaceous materials prepared from a wide low-cost biomass feedstocks and biomass of different origins as activated sludge, algae, animal manures agriculture residues, and forest residues [2]. Derived biochar from these materials are extremely rich in carbon content with unique characteristics as large area, porosity, stability and various functional groups including C–H, –C–O–H, R-COOH, C = O, C–C, C = C, C–O–C, –C–O^- and –C_6H_5 [3]. Biochar materials are generally produced by different pyrolysis procedures in the presence or absence of oxygen atmosphere to favor biomass decomposition in specific environments [4]. Several

✉ Mohamed E. Mahmoud
memahmoud10@yahoo.com

1 Chemical and Petrochemical Engineering Department, College of Engineering and Technology, Arab Academy for Science and Technology and Maritime Transport, Alexandria, Egypt

2 Department of Chemical and Environmental Engineering, Faculty of Chemistry, University of Oviedo, Julián Clavería S/N, 33006 Oviedo, Spain

3 Chemistry Department, Alexandria University, Ibrahimia, P.O. Box 426, Alexandria 21321, Egypt

4 Applied Research Center Thomas Jefferson National Accelerator, Facility and Department of Molecular Biology and Chemistry, Christopher Newport University, Newport News, VA 23606, USA

Published online: 03 April 2023

conditional factors and experimental parameters are well documented to affect the properties of biochar as temperature, pre-treatment method, biomass feedstocks, residence time and others [5]. Therefore, pristine biochars are regarded as good sustainable materials with great attention and interest to employ in a variety of suitable applications including water treatment which are mainly focused on removal of organic and inorganic pollutants [6–8]. Examples of such applications are devoted to the ultrafast and efficient removal of Sm(III) and Cd(II) cations by the use of derived biochar from leaves of Cynara scolymus [9]. The adsorption capability of derived biochar material from banana pseudostem towards methylene blue dye was also reported [10]. A study was illustrated to investigate the impacts of carbonization temperature of derived wheat straw biochar on $Pb^{(II)}$ removal and related mechanism [11]. Maple leaf-derived biochar was recently prepared and applied in adsorptive removal of tetracycline from aqueous solution as an example of organic pharmaceutical pollutants [12]. A series of sustainable banana peel biochars were synthesized using pyrolytic method at temperature 450–750 °C and additionally applied for sorption of acetaminophen and ciprofloxacin drugs under different optimized parameters [13]. Other pristine biochars were also investigated and reported for adsorptive removal of organic and inorganic pollutants from wastewater [14–17]

The low removal capability of biochar materials under specific aqueous conditions for some selected contaminants represents one of the major disadvantages with respect to application for removal of diversiform contaminants. Therefore, this problematic issue was found to limit the utilization of pristine biochars compared to the removal ability of modified ones, especially in high ionic strength wastewater [18]. A number of modified biochar adsorbents, nanosorbents, and biosorbents have been recently designed and effectively implemented in wastewater purification of organic, inorganic and biological contaminants [19–24]. For example, a method was developed to enhance removal of Congo red by three pyrolalized biochar from agro-waste (Acacia auriculiformis) at 500 °C and modified with $CaCl_2$, $AlCl_3$ and $FeCl_3$ as metal salts [25]. Sorption of ciprofloxacin (CIP) and tetracycline (TC) in single- and binary-solute systems was studied by a sponge-like structure of cobalt and gadolinium modified biochar (MBC) and the reported maximum capacities were established as 44.44 and 119.05 mg/g for CIP and TC, respectively [26]. Oxidation with 5% of HNO_3/H_2SO_4 mixture was performed to enhance the long-term oxidative aging of the produced corncob biochar material to improve the adsorptive removal of some nanoplastics as polystyrenes (PSNPs) [27]. Modified biochar materials with lauric acid and iron oxide-were used for oil recovery from water [28] and other modified biochars in various applications were recently reported [29–34].

MB is a cationic dye which is widely used as a dyestuff in various textile and industrial activities. The MB discharged residual amounts from these activities are regarded as potential toxins with carcinogenic impact [35]. On the other hand, lead is a highly toxic and non-biodegradable heavy metal with high bioaccumulation in aquatic systems to generate hazardous effects and health problems [36]. Therefore, polluted wastewater effluents with MB and lead ions must be subjected to prior treatments before disposal into water resources. This may be accomplished by using various chemical, physical and biological approaches via ultrafiltration, reverse osmosis membrane separation, oxidation, biodegradation, and adsorption [37]. Therefore, the current study is planned and designed to investigate and compare the adsorption efficiency and performance of pristine derived nanobiochar from Cynara scolymus leaves (CSNB) versus its modified material with Amberlite cation exchanger (ACE@CSNB). The modified nanobiosorbent was generated via homogenized surface modification of the biochar material with ACE via successive grinding and microwave hydro/solvo/thermo/microwave irradiation approach based on the combination of ACE with CSNB (1:5 mass ratio) in a mixture of distilled water–ethanol-microwave heating (3 min). The surface of ACE@CSNB nanobiosorbent is designed to be homogenously covered with (-SO_3Na) groups to enable adsorptive exchange of cationic pollutants as $Pb^{(II)}$ ions & MB dye from aqueous solution in the presence of optimized experimental parameters.

2 Experimental

2.1 Instrumentations

The employed instruments in this work for measurement of the related spectra of ACE and ACE@CSNB nanobiosorbent are listed and detailed in Table 1. In addition, the zero charge point (pH_{pzc}) of ACE@CSNB nanobiosorbent was experimentally measured by mixing ACE@CSNB with either 0.1 mol L^{-1} HCl or 0.1 mol L^{-1} NaOH and 50 mL of NaCl (0.01 mol L^{-1}) to maintain a range of pH 2–10. These solutions were then automatically shaken for 4 h and left at room temperature for 24 h. To determine the pH_{pzc} of ACE@CSNB nanobiosorbent, a plot between $pH_{initial}$ values against ΔpH ($pH_{final} - pH_{initial}$) was established [38].

2.2 Chemicals and materials

All utilized chemicals in this study were of AR grade and employed without more purification or treatment. The employed cation exchanger is Amberlite resin IR-120 (Na) with particle size 0.30–1.18 mm (14–52 mesh) and in a standard grade purchased from BDH limited, Poole

Table 1 Specifications of characterization and instrumental techniques

Characterization	Instrument	Conditions
FT-IR	BRUKER VERTEX 70 Fourier Transform infrared spectrophotometer	In the range 400–4500 cm^{-1}
SEM	Scanning electron microscopic JSM-6360LA, JEOL Ltd	A carbon tap was used as a substrate for SEM measurements using an ion sputtering coating device (JEOL-JFC-1100E)
EDX	Energy Dispersive X-ray, JSM-lT200, JEOL Ltd	A carbon tap was used as a substrate for EDX measurements. Acceleration voltage 20.00 kV, WD 10.00 mm, Live time 30.00, high vacuum mode
TEM	Transmission electron microscopy, model JEOL JEM-2100F, Japan	Acquiring the images at 80 to 200 kV
TGA	CI Electronics microbalance (MK2-MC5)	TGA was acquired under He atmosphere using temperature range 25–900 °C at 10 °C/min ramp
TPD–MS	Micromeritics TPD-2900 apparatus connected to a Pfeiffer Vacuum-300 mass spectrometer	A 0.10 g biochar sample was maintained in a stream of 2% O_2: 98% He at 50 °C for 30 min, with a flow rate of 50 cm^3/min, and heated from 50 to 950 °C at 10 °C / min
XPS	X-ray photoelectron spectroscopy, Thermo Fisher Scientific, USA	Red copper metal was used as a substrate in the XPS analysis. The XPS was collected on K-ALPHA (Themo Fisher Scientific, USA) with monochromatic X-ray Al K-alpha radiation – 10 to 1350 eV spot size 400 micro at pressure 10–9 mbar with full spectrum pass energy 200 eV and at narrow spectrum 50 eV
XRD	The X-ray diffraction by XRD Shimadzu lab X6100, Japan	The XRD generator worked at 40 kV, 30 mA, and $\lambda = 1$ Å utilizing target Cu-Kα with secondary monochromatic 2-Theta was started at 10° and ended at 80° The diffraction data was recorded with step of 0.02° and a time of 0.6 s at room temperature
UV/ViS spectrophotometer	Ultraviolet/visible spectrophotometer by V-530 JASCO	UV/ViS spectrophotometer in between the range of wavelength from 190 to 1100 nm was used in the absorption measurement
pH-meter	Adwa pH-meter	Standard buffers 4.01, 7.00, and 10.00 were utilized in the calibration of Adwa pH-meter which used in the measurements of solutions pH

England. The Cynara scolymus were purchased from a nearby marketplace. Methylene blue (MB) dye content, ≥ 82%, was received from Sigma-Aldrich Chemical Company, USA. $Pb(CHCOO)_2{\cdot}3H_2O$ (purity = 99%) and disodium ethylenediaminetetraacetate dihydrate (EDTA) (assay > 99.0%) were purchased from El-Nasr Pharmaceutical Chemicals, Egypt. Hydrochloric acid (37%) and sodium hydroxide (98%) were provided from (SD fine Chem. Limited, India). Calcium sulfate ($CaSO_4$ with purity = 97%) and magnesium sulfate heptahydrate ($MgSO_4.7H_2O$ with purity = 98%) were purchased from Adwic company, Egypt. Sodium hydroxide scales (NaOH with purity 96%) and ammonia solution (assay 25%) were purchased from EL-Nasr Pharmaceutical Chemicals, Egypt. NaCl (purity 99.0%), KCl (purity 99.5%), and NH_4Cl (purity 99.0%) were obtained from Riedel-de-Haen, Germany.

2.3 Synthesis methodology

2.3.1 Synthesis of pristine nanobiochar

Synthesis of pristine nanobiochar (CSNB) was prepared from Cynara scolymus leaves as previously reported and according to the following procedure [9]. The collected leaves of Cynara scolymus feedstocks were first treated several times with distilled water to remove impurities, divided into small pieces and then desiccated at 70 °C. The material was heated by a slow heating at 350 °C for 1 h and left to attain to the room temperature. The produced CSNB was washed several times with distilled water and left to dry at 70 °C for 24 h. The CSNB material was collected as a homogeneous powder based on gentle milling and sieving.

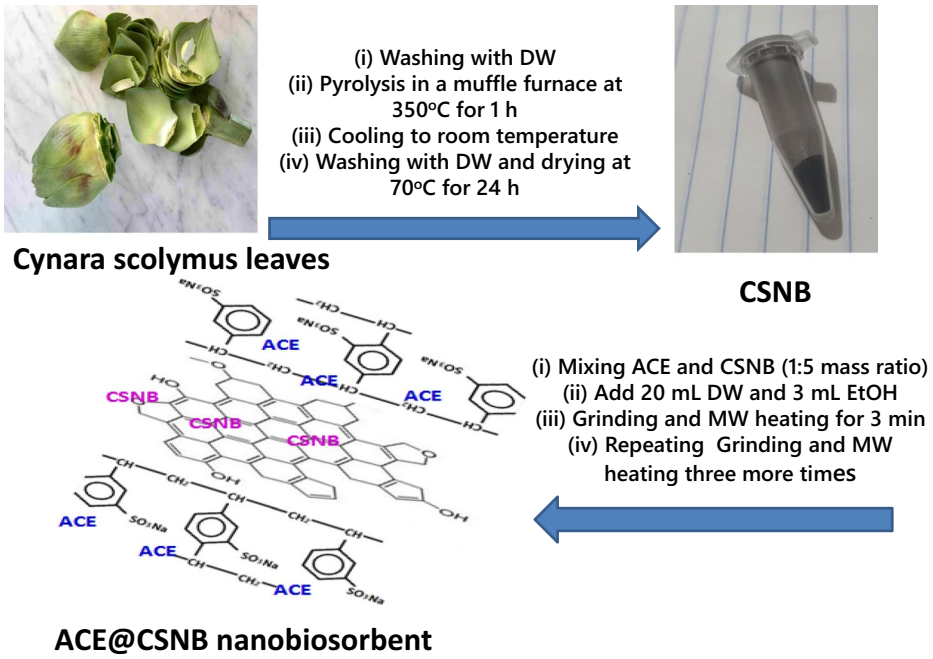

Scheme 1 Schematic diagram for surface coating of ACE on CSNB (CE@CSNB)

2.3.2 Hydro/solvo/thermo/microwave surface modification of ACE on CSNB (CE@CSNB)

Surface modification of Amberlite resin cation exchanger (ACE: IR-120-Na) onto derived Cynara scolymus nanobiochar (CSNB) was accomplished by the combined hydro/solvo/thermo/microwave process using distilled water–ethanol-microwave heating and irradiation. In this procedure, 1.0 g (ACE) was mixed with 5.0 g (CSNB) in a 1:5 mass ratio and this solid mixture was added to 20 mL DW and 3 mL EtOH. The mixture was heavily grinded in a mortar and followed by microwave irradiation heating for 3 min. The produced ACE@CSNB nanobiosorbent was left to cool at room temperature, mixed with 5 mL DW, heavily grinded, irradiated in a microwave for additional 2 min and left to cool. The last steps of mixing, grinding, microwave irradiation and cooling were repeated three more times to ensure complete homogenous microwave surface modification of ACE onto CSNB for the formation of the aimed nanobiosorbent (CE@CSNB) as illustrated in Scheme 1.

2.4 *Adsorption behavior of modified ACE@CSNB nanobiosorbent versus pristine CSNB for $Pb^{(II)}$ & MB pollutants*

The adsorption performance of ACE@CSNB nanobiosorbent versus pristine CSNB towards $Pb^{(II)}$ ions & MB dye pollutants as cationic water contaminants was principally investigated and optimized in the presence of various operational factors. The following experimental protocol was adapted and followed based on using the batch equilibrium method. Stock solutions of 1000 mg L^{-1} MB and 0.1 mol L^{-1} $Pb^{(II)}$ were diluted to the required concentrations using DW. As a general method, a given amount of the examined nanobiosorbent (ACE@CSNB or CSNB) was mixed with either 20 mL MB solution (15 mg L^{-1}) or $Pb^{(II)}$ ions (15 mmol L^{-1}) and mechanically shaken for a certain period of time. At the end of each batch experiment, the investigated nanobiosorbent (ACE@CSNB or CSNB) was isolated by filtration and the residual concentrations of $Pb^{(II)}$ ions & MB dye pollutants were detected by complexometric titration and UV–Vis spectrophotometric determination at $\lambda_{max} = 664$ nm, respectively. The average removal (%R) and equilibrium adsorption capacity (q_e) were then calculated for MB dye & $Pb^{(II)}$ ions pollutants after three times of repeated experiments according to Eqs. (1) and (2), respectively.

$$\text{Removal}(\%R) = \left[\left(C_o - C_e\right)/C_o\right] \times 100 \quad (1)$$

$$q_e = Vx\left(C_o - C_e\right)/W \quad (2)$$

wherein C_o and C_e values represent the starting and final equilibrium concentration for MB (mg L^{-1}) and $Pb^{(II)}$ (mmol L^{-1}), W is the mass of employed biochar and V is the solution volume (L). A number of controlling experimental parameters were testified and optimized including solution biochar dosage, reaction time, initial contaminant concentration, temperature, pH, and medium ionic strength as outlined below.

2.4.1 *Role of biochar mass on removal of $Pb^{(II)}$ & MB pollutants by pristine and modified biochars*

The first investigated factor was related to the impact of biochar mass. In this step, 20 mL of MB (15 mg L^{-1}) was mixed with the selected mass of biochar (5–60 mg), shaken

for 30 min, filtered and the remaining concentration of MB in the filtrate was spectrophotometrically detected at $\lambda_{max} = 664$ nm. The average percentage removal values (%R) were finally computed according to Eq. (1). A 10 mL of $Pb^{(II)}$ ion (15 mmol L^{-1}) was mixed with the selected mass of biochar (5–60 mg) and added in a 50-mL flask. This was shaken (30 min), filtered, and washed (20 mL DW). The residual concentration of $Pb^{(II)}$ in the filtrate was determined against 0.01 mol L^{-1} EDTA using hexamine and xylenol orange indicator. The equilibrium capacity values (q_e) were finally computed according to Eq. (2).

2.4.2 *Role of reaction time on removal of $Pb^{(II)}$ & MB pollutants by pristine and modified biochars*

MB solution (20 mL, 15 mg L^{-1}) was added to the selected mass of biochar (20 mg) and shaken by an automatic shaker for the selected time (5–60 min). These mixtures were filtered, and the remaining concentrations of MB were spectrophotometrically determined at $\lambda_{max} = 664$ nm to calculate the average percentage removal values (%R) of MB as computed according to Eq. (1). A 10 mL of $Pb^{(II)}$ ions (15 mmol L^{-1}) were mixed with the selected mass of biochar (20 mg) in 50-mL measuring flasks. These were automatically shaken for the selected time (5–60 min), filtered and washed with 20 mL DW. The residual concentration of $Pb^{(II)}$ in the filtrate was then determined against 0.01 mol L^{-1} EDTA to identify the equilibrium adsorption capacity)q_e) according to Eq. (2).

2.4.3 *Role of initial contaminant concentration on removal of $Pb^{(II)}$ & MB by pristine and modified biochars*

The role of initial concentration of investigated MB pollutant was studied by using various dye concentrations in the range 2–15 mg L^{-1}. In this study, 20 mL MB solutions were mixed with the selected mass of biochar (20 mg) and shaken (30 min). The mixtures were filtered, and MB were determined at $\lambda_{max} = 664$ nm to calculate (%R) of MB from Eq. (1). Ten milliliter solution of $Pb^{(II)}$ ion (5–50 mmol L^{-1}) were mixed with the selected mass of biochar (20 mg) in 50-mL measuring flasks and shaken by automatic shaker for the selected time (30 min). These mixtures were filtered, washed with 20 mL DW and determined by EDTA (0.01 mol L^{-1}) to characterize the q_e values from Eq. (2).

2.4.4 *Role of reaction temperature on removal of $Pb^{(II)}$ & MB pollutants by pristine and modified biochars*

The role of reaction temperature on $Pb^{(II)}$ ions & MB dye removal was investigated at temperature range (25–60 °C). In this step, 20 mL MB solutions (15 mg L^{-1}) were mixed with the selected mass of biochar (20 mg) and shaken under a thermostat automatic shaker at the defined reaction temperature for the selected time (30 min). The mixtures were filtered, and the remaining concentrations of MB were spectrophotometrically determined at $\lambda_{max} = 664$ nm. Solutions of $Pb^{(II)}$ ions (10 mL, 15 mmol L^{-1}) were mixed with the selected mass of biochar (20 mg) and automatically shaken for 30 min under the specified temperature, filtered, washed with 20 mL DW, and the residual $Pb^{(II)}$ was determined as above.

2.4.5 *Role of solution pH on removal of $Pb^{(II)}$ & MB by pristine and modified biochars*

The role of solution pH on MB (%R) and lead ions (q_e) was investigated at pH range (pH 2–10) and (pH 2–6), respectively, by using 20 mL of MB solutions (15 mg L^{-1}) and 10 mL of $Pb^{(II)}$ ions (15 mmol L^{-1}). These were mixed with the selected mass of biochar (20 mg) and shaken at room temperature for the selected time period (30 min). The reaction mixtures were filtered and the remaining concentration of MB in the filtrate was spectrophotometrically determined at $\lambda_{max} = 664$ nm to figure out (%R) values from Eq. (1) and the residual $Pb^{(II)}$ was then determined by 0.01 mol L^{-1} EDTA to identify the q_e values from Eq. (2).

2.4.6 *Role of medium ionic strength on removal of $Pb^{(II)}$ & MB by pristine and modified biochars*

The influence of ionic strength on the adsorption behavior and removal values of MB (%R) and lead ions (q_e) by CSNB and ACE@CSNB was carried out by the addition of different masses of sodium chloride electrolyte (10–100 mg). The applied mass of NaCl was added to 20 mg of biochar material and mixed with 20 mL of MB solutions (15 mg L^{-1}) or 10 mL of $Pb^{(II)}$ ions (15 mmol L^{-1}). These solutions were shaken at room temperature for the selected time period (30 min), filtered, and the remaining concentration of MB was determined at $\lambda_{max} = 664$ nm to figure out (%R) values using Eq. (1) and the residual $Pb^{(II)}$ was determined by 0.01 mol L^{-1} EDTA to identify (q_e) values using Eq. (2).

2.4.7 Recyclability and reusability of ACE@CSNB nanobiosorbent

Recyclability and reusability of ACE@CSNB nanobiosorbent after its initial utilization in removal of $Pb^{(II)}$ & MB pollutants were additionally performed according to the following procedure. The loaded pollutants on the surface of ACE@CSNB were subjected to treatment with 50 mL (0.1 mol L^{-1} HCl) for 1 h. The regenerated solid materials were treated with DW to the neutral pH condition and finally dried at 60 °C. The regenerated ACE@CSNB nanobiosorbent was applied to further remove $Pb^{(II)}$ & MB pollutants.

The above procedure was repeated to reach to five recycled nanobiosorbents and the q_e and %R values of $Pb^{(II)}$ & MB dye were determined, respectively.

2.5 *Real water sample treatment from $Pb^{(II)}$ & MB by ACE@CSNB*

The application process of ACE@CSNB nanobiosorbent in removal of both $Pb^{(II)}$ ions & MB dye pollutants from water samples (industrial waste, sea and tap water matrices) were investigated by the batch approach via spiking the examined water samples (100 mL) with 10 and 15 mg L^{-1} pollutant. These samples were then mixed with 50 mg ACE@CSNB and shaken for 60 min. The percentage removal values (%R) of $Pb^{(II)}$ ions & MB dye pollutants from various water samples were characterized and fulfilled as mentioned above.

3 Results and discussion

3.1 Characterization of pristine CSNB and ACE@CSNB nanobiosorbent

The pristine nanobiochar (CSNB) was prepared via a simple heating method by heating clean and dry leaves of Cynara scolymus feedstocks at 350 °C for 1 h and followed by washing with distilled water and drying at 70 °C. The surface of produced CSNB material was further homogenized with Amberlite cation exchanger IR-120 (Na) (ACE) to generate the modified ACE@CSNB nanobiosorbent with surface modified R-SO_3^- as the reactive functional group for effective binding with cationic pollutants as MB dye and $Pb^{(II)}$. The synthetic methodology was based on the combination of hydro-solvo-thermo process by using distilled water–ethanol-microwave heating and irradiation. The schematic diagram for preparation of ACE@CSNB nanobiosorbent is illustrated in Scheme 1. The generated CSNB and ACE@CSNB nanobiosorbents were characterized by a number of techniques as FT-IR, SEM, TEM, EDX, XPS, TGA, TPD-MS and surface area as discussed in the following sections.

3.1.1 FT-IR characterization of pristine CSNB and modified ACE@CSNB

Physicochemical characterization of CSNB and ACE@CSNB by FT-IR analysis was aimed in this study to recognize and refer to the major active functional groups loaded on the biochar surface. The FT-IR of pristine biochar (CSNB) is shown in Fig. 1 a and denotes to the appearance of a number of functional groups including a broad band at 3200–3430 cm^{-1} for the vibration of O–H groups. Several other peaks were characterized and evident at 2930 and 2955 cm^{-1} (aliphatic/aromatic C–H stretching), 1625 cm^{-1} (C = O stretching vibration), 1590 cm^{-1} (C = C vibrations), 1115–1200 cm^{-1} (pyrone group), and 750 cm^{-1} (C–H out of-plane deformation in benzene ring) [9]. The same characteristic peaks could be also detected in the FT-IR of ACE@CSNB nanobiosorbent due to the close aliphatic and aromatic nature in the modified biochar as illustrated in Fig. 1 b. However, the characteristic sulfonate peak (R-SO_3^-) is characterized by stretching modes at 1140–1250 cm^{-1} and 1030–1070 cm^{-1} for R-SO_3^- with S = O [39] to confirm the successful surface modification by pristine biochar (CSNB) with Amberlite cation exchanger IR-120 (Na) (ACE) for the formation of the aimed ACE@CSNB nanobiosorbent.

3.1.2 SEM/EDX characterization of pristine CSNB and modified ACE@CSNB

The surface morphology of the as-generated pristine CSNB and modified ACE@CSNB nanobiosorbents was acquired by the SEM technique. The SEM images of CSNB and ACE@CSNB are represented in Fig. 2 a and b, respectively at the same comparable magnification order (35,000 ×). It is clear that the pristine CSNB are homogenously distributed in spherical nanoparticles with the nanoscale range (18.74–21.85 nm). On the other hand, the SEM-image of ACE@CSNB nanobiosorbent is also providing good evidence for the similarity and homogeneity of nanoparticle distribution in the range (18.74–23.70 nm) to confirm somewhat partial increase in the produced nanoparticles upon loading of ACE on the surface of CSNB. In addition, this behavior led to close attachment of the particles compared to those in the SEM-image of pristine CSNB. Figure 1S (Supplementary material) is also provided to give more evidence for the surface coverage and modification of pristine CSNB biochar with ACE at a magnification order (15,000 ×).

The EDX diagrams of CSNB and ACE@CSNB biochar materials are shown in Fig. 2 c and d and refer to the presence of carbon (81.85%) and oxygen (17.32%) as the two dominant elements in CSNB biochar. The elemental composition was also contributed by other elements as calcium, sodium, potassium as previously described [9]. Similarly, the modified ACE@CSNB biochar was also characterized with high contents of both carbon (81.98%) and oxygen (17.00%) along with sodium (0.48%) and sulfur (0.54%) due to the contribution of sodium sulfonate group ($-SO_3^-\ Na^+$).

3.1.3 XPS of pristine CSNB and modified ACE@CSNB

The X-ray photo-electron spectroscopy (XPS) analysis was acquired for pristine CSNB and modified ACE@CSNB before and after removal of $Pb^{(II)}$ ions as shown in Fig. 2e(i–iii) and f(i–iii), respectively. As depicted in Fig. 2 e(i), the XPS of pristine CSNB refers mainly to the existence of two sharp peaks corresponding to the carbon and oxygen

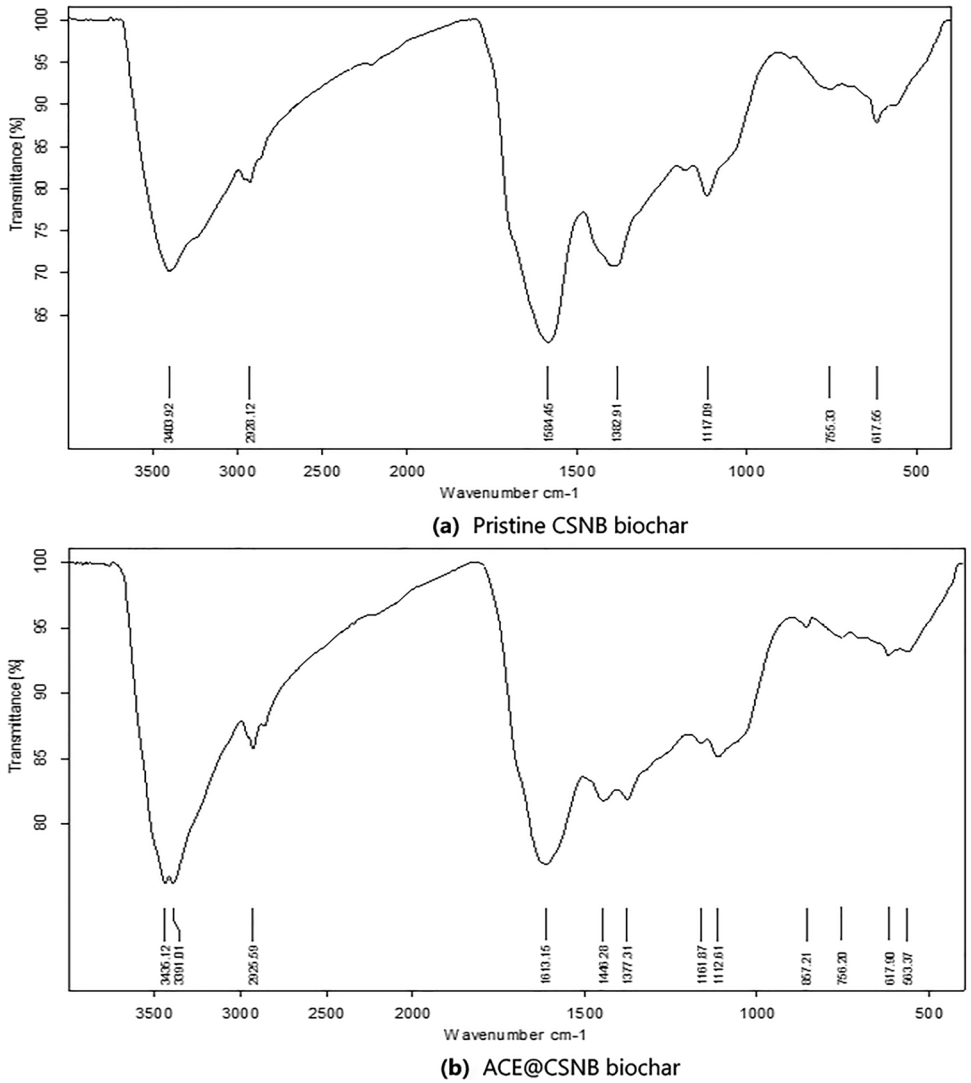

Fig. 1 FT-IR characterization of **a** pristine CSNB and **b** ACE@CSNB nanobiosorbent

elements, respectively. The first assigned peak in pristine CSNB is associated with binding energies at ~ 286 eV for C1s-π* transition due to COH, phenolic C, C = O, ketonic C; R-(C = O) or substituted aromatic C, ~ 287 eV for C1s-3p-σ* due to C-H, aliphatic C of CH_3, CH_2 and CH bonds and ~ 289 eV for C1s-π* due COOH, carboxylic C; COO, C = O carbonyl C and C-O, moieties to confirm the presence of these carbon functional groups. The second peak in Fig. 2 e(i) is directly related to the oxygenated functional groups (O1s) at compatible binding energies of C = O (~ 531 eV) and C-O (~ 534 eV) and O–H (532 eV) [40]. Similarly, and as represented in Fig. 2 f(i), the modified ACE@CSNB was also identified to exhibit two identical peaks at 286–289 eV (C1s-π* and C1s-3p-σ*) and 531–535 eV (O1s) which are correlated to binding energies of carbon moiety and oxygenated functional groups. On the other hand, Fig. 2 e(ii) and f(ii) are directly representing the XPS spectra of pristine CSNB and modified ACE@CSNB after adsorption of $Pb^{(II)}$ ions. It is evident that more characteristic peaks were produced due to surface adsorption of $Pb^{(II)}$ on both biochar materials. It was detected that the binding energies of these peaks showed different ratio of distribution in O = C-O and C-O with slight shifts due to adsorption of Pb^{2+} ions on the surface of pristine CSNB and modified ACE@CSNB [41]. Figure 2 e(iii) and f(iii) were acquired from the two general Fig. 2 e(i) and f(i), respectively which are characterized by two adjacent and identical peaks at 132.5–137.8 eV and 138.1–144.2 eV to confirm the presence of different functionalized lead groups as Pb-OH, Pb–O-C = O, Pb–O-C, and Pb–O based on the main dominant binding forms with OH, COO, CO, and O functional groups, respectively [42].

3.1.4 TGA of pristine CSNB and modified ACE@CSNB

Thermal gravimetric analysis (TGA) of CSNB was studied under He atmosphere and compared with modified ACE@CSNB under temperature range from 25 to 900 °C using 10 °C/min ramp and their related thermograms are illustrated

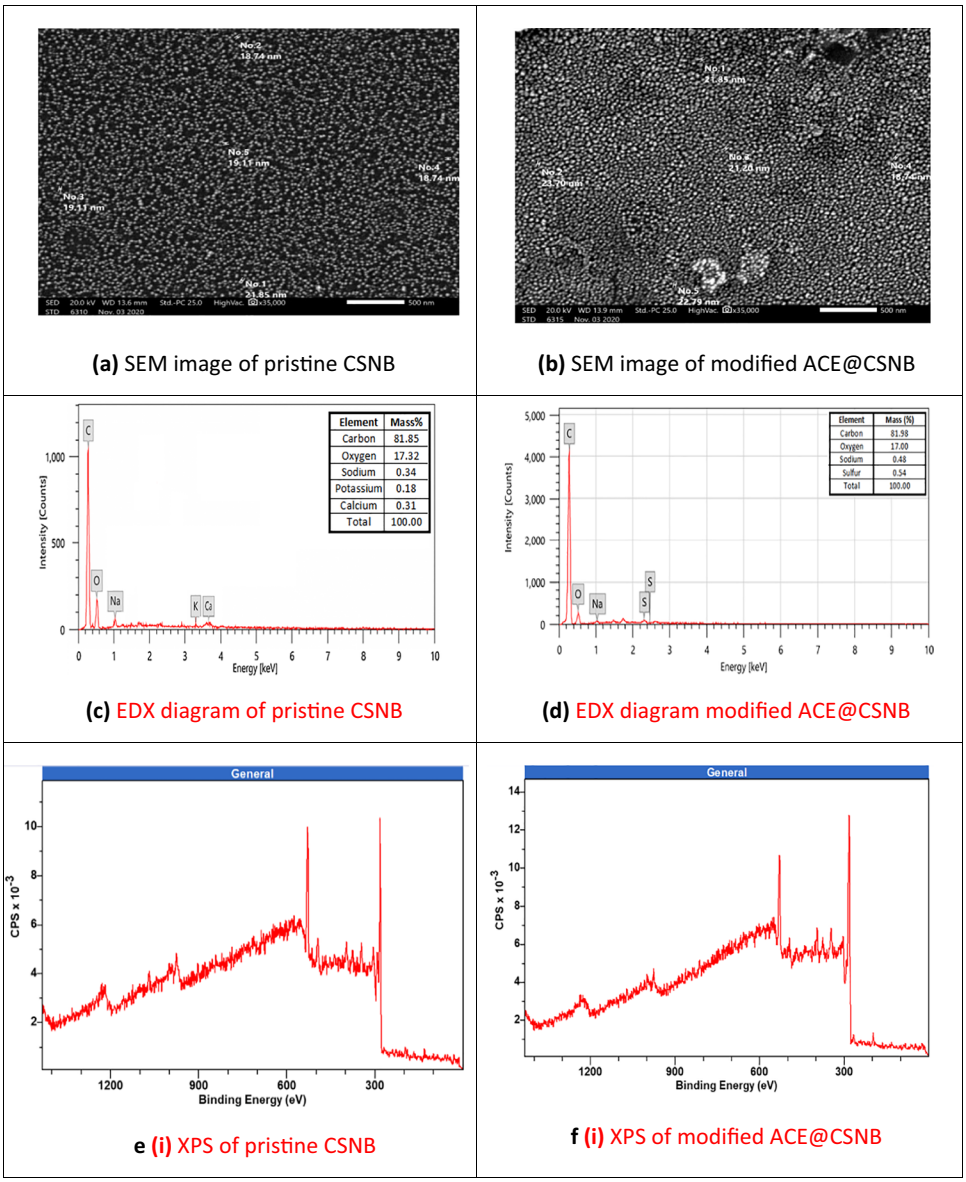

Fig. 2 SEM/EDX/XPS/TGA/TPD-MS of pristine CSNB and ACE@CSNB nanobiosorbent

in Fig. 2 g and h, respectively. The TGA thermogram of CSNB is characterized by five decomposition stages at 20–100, 100–340, 340–540, 540–740, and 740–900 °C which are related to the release of moisture and other decomposed organic moieties with percentage losses values corresponding to 6.2, 6.1, 17.5, 5.3, and 15.2%, respectively. The sum of total decomposed material is only 50.3% up to heating temperature at 900 °C to reveal that 47.7% of this pristine CSNB material is highly thermally stable. Similarly, the thermogram of modified ACE@CSNB was identified with five decomposition stages, but at different temperatures and percentage losses. As listed in Fig. 2 h, these five steps were produced at 20–60 °C (loss = 6.0%), 60–220 °C (loss = 4.0%), 220–460 °C (loss = 18.2%), 460–700 °C (loss = 11.5%), and 700–900 °C (loss = 16.4%). Therefore, the total percentage loss from the modified ACE@CSNB was found 56.1%, while 43.9% as the residual amount. Such configured results confirm the successful loading of ACE on the surface of CSBC. However, the loaded organic material on CSNB was identified to contribute by a decrease in thermal stability via 5.8%.

3.1.5 TPD–MS of pristine CSNB and modified ACE@CSNB

Coupling of temperature programmed desorption technique with mass spectrometer (TPD–MS) provides a valuable and complementary data for TGA based on the detection of some evolved gasses according to their m/z values which help in characterization of the different functional groups in pristine CSNB and modified ACE@CSNB [43]. Therefore, the incorporated surface functionalization onto pristine CSNB and modified ACE@CSNB were investigated by TPD-MS experiments under evacuated condition for 30 min at room temperature to yield important and valuable data as

Fig. 2 (continued)

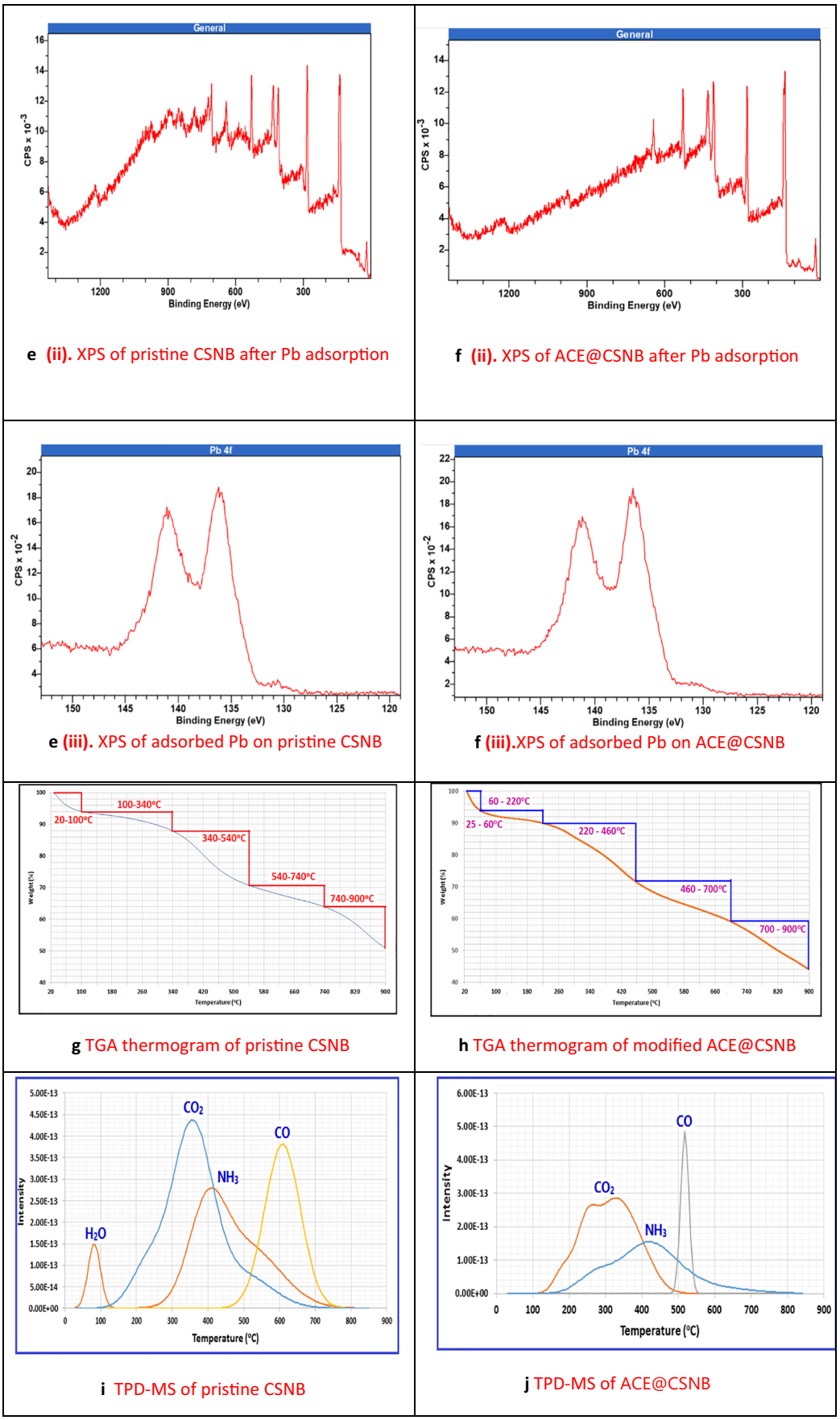

represented in Fig. 2 i and j, respectively. The temperature was started at 50 °C and increased to a maximum value at 750 °C using a 10 °C min^{-1} heating rate. The TPD–MS diagram of pristine CSNB is characterized by the presence of four different peaks with the maximum intense related one to CO_2, which is followed by CO, NH_3 and finally, the lowest peak is assigned to H_2O with detected m/z values at 44, 28, 17, and 18 amu, respectively. The observed CO_2 may be produced as a result of the thermal decomposition of various functional groups as carboxyl, lactonic, and acid anhydride groups, while CO is generally produced from some oxygenated carbon groups as carbonyl, phenolic, pyrone and quinine moiety as previously reported [44]. It is evident from the TPD–MS diagram of pristine CSNB that the thermal decomposition and evolution of CO_2 and CO gases were initiated and ended at two different heating temperature ranges and their peak maxima were detected at 360 and 610 °C, respectively. This trend could be interpreted by the facile evolution of CO_2 and CO from different amounts of carboxyl and phenol–carbonyl groups, respectively. The NH_3 peak was produced mainly at 420 °C as a result of thermal decomposition of some nitrogenated contents in the pristine biochar as previously reported [45], while the loss of H_2O was mainly detected at 85 °C to confirm the presence of adsorbed or bonded water molecules. On the other hand, Fig. 2 j illustrates the presence of three TPD-MS peaks in modified ACE@CSNB and these are related to the evolution of CO_2, NH_3 and CO gases at temperatures 320, 415, and 510 °C, respectively to refer to the successful immobilization and loading of ACE on the surface of pristine CSNB. It is evident also that the related peak to CO became more intense and sharp due to the increase in phenolic moiety, while the two related peaks to CO_2 and NH_3 were weakened, if compared to their intensity in Fig. 2 i of the pristine CSNB. Moreover, the characteristic peak of H_2O was disappeared from the TPD-MS diagram of modified ACE@CSNB.

3.1.6 BET-surface properties of pristine CSNB and modified ACE@CSNB

The collected BET data including the mean pore size, surface area, and total pore volume of CSNB and ACE@CSNB biochar materials were measured and characterized by using the standard BET method. The pristine CSNB exhibited a surface area value corresponding to 129.8 $m^2\ g^{-1}$, while the modified ACE@CSNB biochar provided 50.1 $m^2\ g^{-1}$ to refer and confirm to the successful production of this material according to the particle size decrease via surface modification and loading of ACE on the surface of CSNB. In addition, the characterized pore volumes were identified as 1.206×10^{-3} $cm^3\ g^{-1}$ (CSNB) and 2.801×10^{-2} $cm^3\ g^{-1}$ (ACE@CSNB) to refer to higher pore volume in the modified biochar. Moreover, the mean pore size of CSNB was detected as 3.717×10^{-2} nm, while the modified ACE@CSNB biochar exhibited high pore size corresponding to 2.238 nm to categorize the modified biochar as a typical mesoporous material because it is in the range between 2 and 50 nm [46]. Finally, the observed decrease in the particle size and surface area with the increase of total pore volume and mean pore size in the modified ACE@CSNB biochar are directly refereeing to the successful immobilization and functionalization of CSNB with ACE by the employed hydro/solvo/thermo microwave approach.

3.2 *Removal optimization of $Pb^{(II)}$ ions & MB dye pollutants*

Adsorption is now recognized and categorized as an effective and economic methodology for removal of miscellaneous biological and chemical pollutants from wastewater. Such interest is mainly relying on several incorporated parameters and characteristics of the adsorbents including flexibility in design, simplicity in operation, cost effectiveness, sustainability, regeneration, reuse and others [47, 48]. On the other hand, adsorptive removal of $Pb^{(II)}$ ions & MB dye pollutants from water by different adsorbents as CSNB and ACE@CSNB biochar materials are known to be heavily dependent on several important controlling factors as biochar dosage, contact time, initial pollutant concentration, reaction temperature, ionic strength and solution pH [49]. These factors were extensively studied and evaluated in order to identify and optimize the sorption conditions for possible removal of $Pb^{(II)}$ ions & MB dye as important examples of organic and inorganic pollutants.

3.2.1 The impact and role of biochar mass

Dosage is an important parameter in sorption studies because it determines the removal efficiency of adsorbent with the interacting pollutant [50]. To perform this evaluation, various amounts of CSNB and ACE@CSNB were applied for MB dye and $Pb^{(II)}$ pollutants (5–60 mg) with the aim of comparing of their behaviors towards $Pb^{(II)}$ ions & MB dye pollutants. The average values of triplicate investigation were calculated and the results (Table 2) refer to the concluded percentage removal efficiency (%R) of MB and metal capacity (q_e) of $Pb^{(II)}$ ions. It is evident from the outlined data that a gradual increasing order was observed in the removal efficiency (%R) from 80 to 93% by increasing the ACE@CSNB dosage from 5 to 20 mg using 15 mg L^{-1} of MB with an established equilibrium and saturation condition at mass ≥ 20 mg. This refers to the possible incorporated homogeneity and similarity in the surface of modified ACE@CSNB nanobiosorbent. On the other hand, the performance of CSNB towards removal of MB (15 mg L^{-1}) was completely different as listed in Table 2. The values were

Table 2 Comparison of MB dye and Pb(II) removal by different masses of CSNB and ACE@CSNB

Initial Concentration	Biochar	Percent removal (%R) ± 0.7%) of MB dye at different masses (mg)*						
		5	**10**	**20**	**30**	**40**	**50**	**60**
15 mg L^{-1} MB dye	**ACE@CSNB**	81	87	93	93	93	93	93
	CSNB	88	90	89	89	87	85	87
Pollutant	**Biochar**	**Metal capacity (μmol g^{-1} ± 1.0%) of Pb(II) at different masses (mg)****						
		5	**10**	**20**	**30**	**40**	**50**	**60**
15 mmol L^{-1} Pb(II)	**ACE@CSNB**	2673	1740	995	735	591	497	414
	CSNB	1181	777	404	342	295	242	236

*%R values are the average of triplicate run with ± **0.7%**

μmol g^{-1} capacity values are the average of triplicate run with ± **0.5%

found inconsistent by going up and down due to possible less homogeneity and aggregation in the surface of CSNB.

The results of the adsorptive capacity values (μmol g^{-1}) by ACE@CSNB nanobiosorbent for removal of $Pb^{(II)}$ ions were also compared with CSNB as compiled in Table 2 based on the average values of triplicate investigation. It is evident that the related values of ACE@CSNB nanobiosorbent were much higher than those concluded by CSNB to refer to the contribution of loaded sulfonate ($–SO_3^-$) anion which facilitated and enhanced the direct cation exchange reaction and binding with $Pb^{(II)}$ ions. The maximum adsorptive capacity values (μmol g^{-1}) were established as 2673 μmol g^{-1} and 1181 μmol g^{-1} by ACE@CSNB and CSNB, respectively. The explanation for this is directly related to the higher biochar dosage, which afford a greater availability of exchangeable sites for $Pb^{(II)}$ ions via exposure of more active sites for binding with the biochar surface. Moreover, the adsorptive capacity values were identified higher at lower biochar dosage due to the increased metal to biochar ratio in the contact solution [51].

Therefore, the role of Amberlite cation exchanger surface loading on CSNB for the formation of more efficient ACE@CSNB nanobiochar is clear with respect to increasing the capacity value via incorporated homogeneity and similarity of surface functional groups. Finally, the optimum mass (20 mg) of either ACE@CSNB or CSNB was used in the following optimization factors for MB dye and $Pb^{(II)}$ ions.

3.2.2 The impact and role of reaction time

The impact of reaction time utilizing the batch technique is known to play a critical role in the adsorption and removal process of various pollutants. Moreover, adsorption technique is a time-dependent process, and accordingly, it is important to characterize the pollutant removal rate for the sake of future design of wastewater treatment plants [52]. The importance of this factor comes from the need for identification and comparison of the optimum time which favors the highest (%R) and (q_e) values for both MB and $Pb^{(II)}$ pollutants by the modified ACE@CSNB and pristine CSNB nanobiosorbents. However, the reaction contact time is characterized as the period of contact between the adsorbent and the solution mixture. Therefore, the effect of contact time on the removal processes of both MB and $Pb^{(II)}$ cations onto ACE@CSNB nanobiosorbent was studied in this work and compared with CSNB using 15 mg L^{-1} and 15 mmol L^{-1}, respectively in the presence of various time intervals (5–60 min) under optimum mass condition (20 mg). The illustrated data in Fig. 3 a and b for MB and $Pb^{(II)}$ pollutants as expressed by the values (%R) and (q_e) for both MB and $Pb^{(II)}$, respectively versus contact time. The concluded average values of triplicate determination of both contaminants refer to the superiority of modified ACE@CSNB nanobiosorbent compared to the pristine CSNB. The detected values (%R) were found 94% and 83% for MB by ACE@CSNB and CSNB to refer to the played role and impact of the loaded sulfonate anion ($–SO_3^-$) in enhancement of the direct reaction and binding with MB molecules. In addition, the stable adsorption rates were mainly attributed to the ease in surface binding between MB and both biochar materials. It is also evident from the graphed data that 20–30 min was sufficient as a contact time to favor reaching to the steady condition by both modified and pristine biochar materials to confirm the rapidness in binding process between the surface groups and pollutants [53]. The same trend was also characterized as illustrated in Fig. 3 b for the superior adsorption of $Pb^{(II)}$ onto ACE@CSNB nanobiosorbent when compared to the pristine CSNB. However, because the concentration of $Pb^{(II)}$ was high (15 mmol L^{-1}), the removal capacity values of $Pb^{(II)}$ onto ACE@CSNB was found steady as 1275 μmol g^{-1} at the time period between 5 and 20 min, then increased to 1320 μmol g^{-1} at 30 min and finally reached to the maximum value as 1336 μmol g^{-1} at 40–60 min.

The outlined data of MB and $Pb^{(II)}$ pollutants removal onto the pristine CSNB biochar and modified ACE@CSNB biochar were also evaluated by three different kinetic models (intraparticle diffusion, *pseudo*-first-order, and *pseudo*-second-order) to identify the possible acting adsorption mechanism [54]. According to the intraparticle diffusion model, the computed R^2 values of MB dye and $Pb^{(II)}$ pollutants

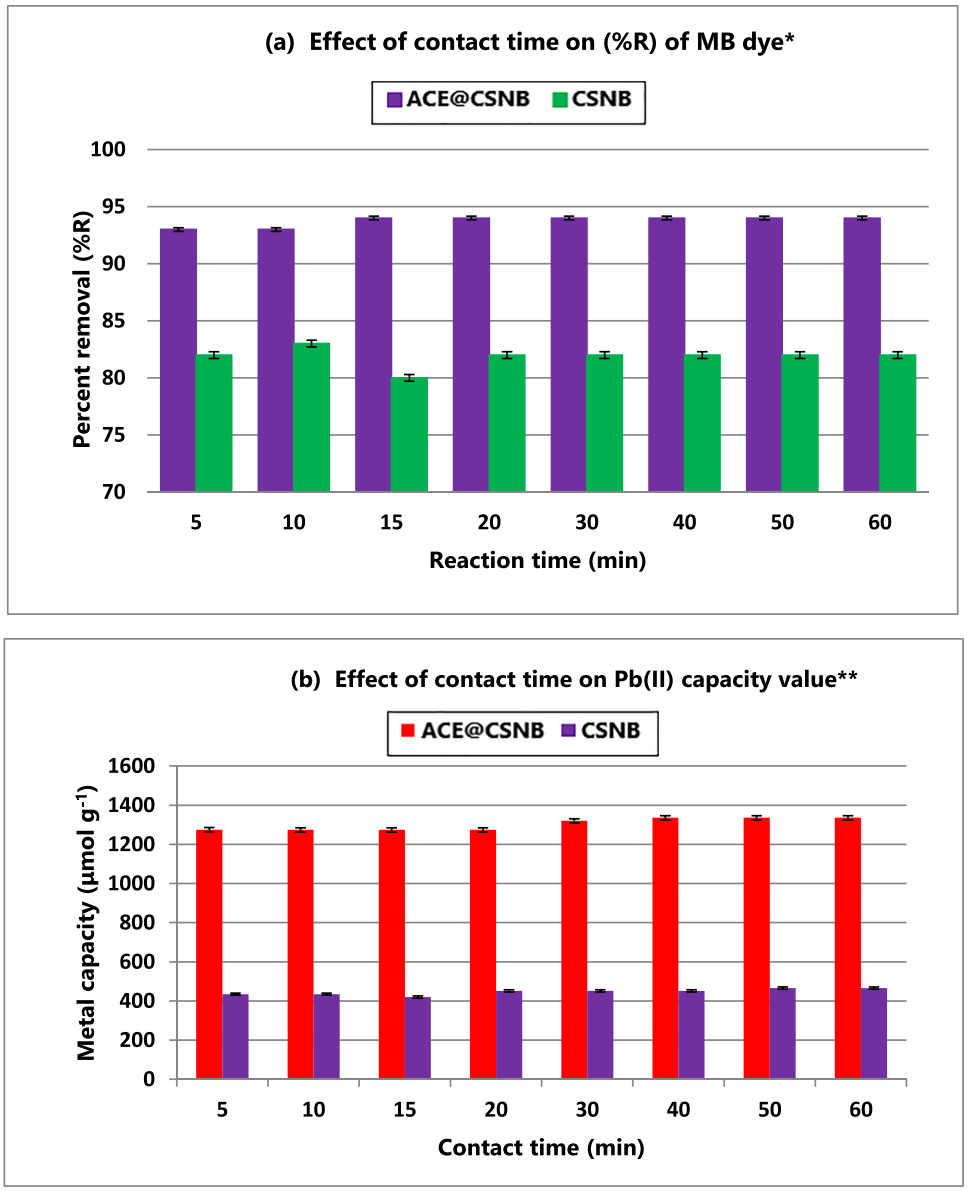

Fig. 3 Comparison of MB dye and Pb(II) removal at different contact times (min)

were characterized in the range 0.958–0.967 and 0.988–990, respectively using both biochars to reveal that this model was invalid to describe the adsorptive removal of MB dye and $Pb^{(II)}$ pollutants onto the pristine CSNB biochar and modified ACE@CSNB biochar. In addition, the *pseudo*-first order model provided also poor correlation coefficients $R^2 = 0.935$ and 0.895 for MB dye and $Pb^{(II)}$ pollutants, respectively using pristine CSNB and $R^2 = 0.952$ and 0.965, respectively by ACE@CSNB biochar to confirm invalidity of this model. Finally, the *pseudo*-second order model confirmed excellent $R^2 = 0.997$ and 0.993 for MB dye and $Pb^{(II)}$, respectively, using CSNB and $R^2 = 0.999$ and 0.998 for MB dye and $Pb^{(II)}$, respectively, by ACE@CSNB biochar to certify that the suggested adsorption reaction mechanisms are mainly based on chemical binding between these two pollutants with both the pristine CSNB biochar and modified ACE@CSNB biochar [55]. Finally, to confirm the chemical binding between the two pollutants and modified biochar, the adsorbed $Pb^{(II)}$ ions and MB dye onto ACE@CSNB were subjected to analysis by FT-IR as shown in Fig. 2S(a) and (b), respectively (Supplementary material). It is evident that several sharp characteristic peaks were produced in the region between 1000 and 1600 cm^{-1} to account for the possible adsorptive chemical binding of $Pb^{(II)}$ ions to the surface of ACE@CSNB as represented in Fig. 2S(a). This behavior may be interpreted on the basis of coordinate bond formation between $Pb^{(II)}$ ions and various active oxygenated donor atoms onto ACE@CSNB in addition to an ion-pair interaction mechanism between the two reacting species as represented in Scheme 2. The same observation is also evident

Scheme 2 Bonding of MB dye and Pb(II) to ACE@CSNB

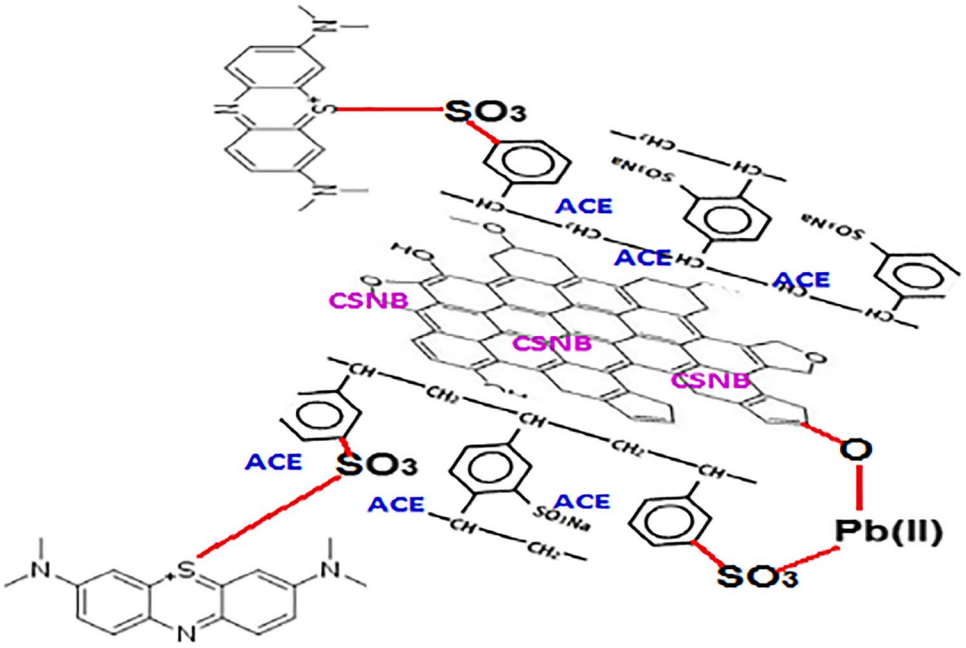

in Fig. 2S(b) by providing other additional characteristic peaks which are responsible for the possible binding of MB dye molecules to the surface of ACE@CSNB via chemical ion-pair formation as represented in Scheme 2.

3.2.3 *The impact and role of initial $Pb^{(II)}$ ions & MB dye concentration*

The impact and role of pollutant concentration is representing another important factor to demonstrate and compare the adsorption trends by the modified ACE@CSNB nanobiosorbent versus pristine CSNB in the presence of different concentrations of the two investigated pollutants, MB dye and $Pb^{(II)}$ ions [56]. This study was performed by using 20 mg of biochar material in 30-min shaking time. The selected concentrations of MB were in the range 2–15 mg L^{-1}, while those of $Pb^{(II)}$ were adjusted at 5–50 mmol L^{-1}. The represented results in Fig. 4 a and b clarify the adsorption behaviors of MB dye and $Pb^{(II)}$ by ACE@CSNB versus CSNB. Gradual increasing orders in the related values to percent MB removal (%R) and $Pb^{(II)}$ capacity (q_e) were evident by increasing the initial contaminant concentration from 2 to 15 mg L^{-1} and 5 to 50 mmol L^{-1}, respectively. The highest (%R) values for MB were referred as 94 and 83% upon using 15 mg L^{-1} and the maximum capacities (q_e) of $Pb^{(II)}$ were 3885 and 3833 µmol g^{-1} by using 50 mmol L^{-1} of $Pb^{(II)}$ onto ACE@CSNB and CSNB, respectively. Such increase in the values of (%R) and (q_e) at higher pollutant concentration is mainly correlated to the existence of high ratio of adsorbate ions versus nanobiosorbent active sites [57]. Moreover, the characterized removal values of MB dye and $Pb^{(II)}$ by ACE@CSNB were found higher than those related to CSNB to confirm the role of loaded sulfonate anion ($-SO_3^-$) in improving and facilitating the direct cation exchange reaction and binding with both MB and $Pb^{(II)}$ cations.

The collected results from this factor was also evaluated by three isotherm models (Freundlich, Dubinin–Radushkevich (D-R) and Langmuir,) to figure out the best fitting model for adsorptive removal of MB dye and $Pb^{(II)}$ onto the pristine CSNB and modified ACE@CSNB biochars [58]. The adsorption Freundlich isotherm provided moderately high correlation according to R^2 values 0.977–985 and 0.980–0.991 for MB dye and $Pb^{(II)}$, respectively using CSNB and ACE@CSNB. Based on the Dubinin–Radushkevich (D-R) isotherm model, the characterized R^2 values of MB dye and $Pb^{(II)}$ pollutants were found to correspond to 0.886–0.867 and 0.751–0.827, respectively using both biochars to reveal that this model was invalid to describe the adsorptive removal of MB dye and $Pb^{(II)}$ pollutants onto the pristine CSNB biochar and modified ACE@CSNB biochar. Finally, the Langmuir adsorption isotherm exhibited excellent correlation R^2 values = 0.997–0.999 and 0.994–0.999 for MB dye and $Pb^{(II)}$, respectively, using CSNB and ACE@CSNB biochars to refer that the adsorption removal mechanism of MB dye and $Pb^{(II)}$ on the two investigated biochars is related to monolayer chemical bond formation on homogeneous surfaces without self-interaction between the contaminants particles [59].

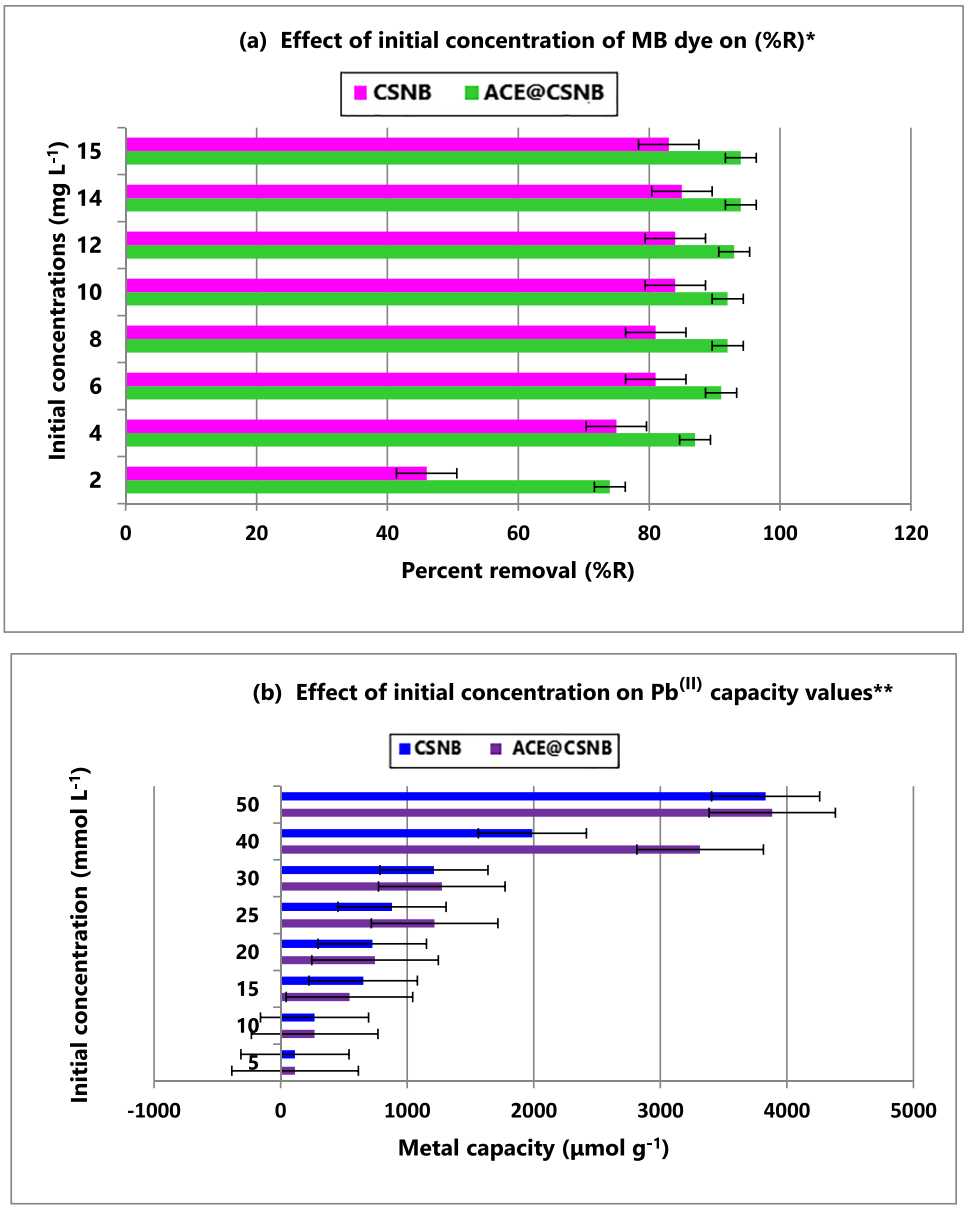

Fig. 4 Comparison of MB dye and Pb(II) removal at different initial pollutant concentrations

3.2.4 The impact and role of reaction temperature

The impact and role of temperature factor is generally applied to figure out and follow-up the variation in adsorption process in the presence of different reaction temperatures to represent a good measure for the nature of the adsorption process as either endothermic or exothermic [60]. This study was followed up by changing the reaction temperature from 25 to 55 °C using a thermostated shaker at 30 min in the presence of 20 mg of either ACE@CSNB or CSNB, while he selected concentrations of $Pb^{(II)}$ ions & MB dye pollutants were 15 mg L^{-1} and 15 mmol L^{-1}, respectively. The illustrations in Fig. 5 a and b refer to the adsorption behaviors of the investigated MB dye and $Pb^{(II)}$ pollutants, respectively by ACE@CSNB versus CSNB. As demonstrated in Fig. 5 a for removal of MB by ACE@CSNB, a slight detected increase in the percentage removal values (R%) from 95% (25–35 °C) to 97% (40–55 °C) to confirm less dependence on reaction temperature. However, ACE@CSNB was identified to react very fast with MB to reach the equilibrium condition at room temperature. On the other hand, removal of MB by pristine CSNB, was found to increase from 87 to 94% by increasing the reaction temperature from 25 to 55 °C to refer to its different behavior when compared to the modified biochar, ACE@CSNB. The comparison of removal efficiency of $Pb^{(II)}$ by ACE@CSNB versus CSNB as expressed in µmol g^{-1} values are plotted in Fig. 5 b. The capacity values of $Pb^{(II)}$ ions by ACE@CSNB and CSNB were identified to increase from 528 to 637 µmol g^{-1} and from 466 to 544 µmol g^{-1} by increasing

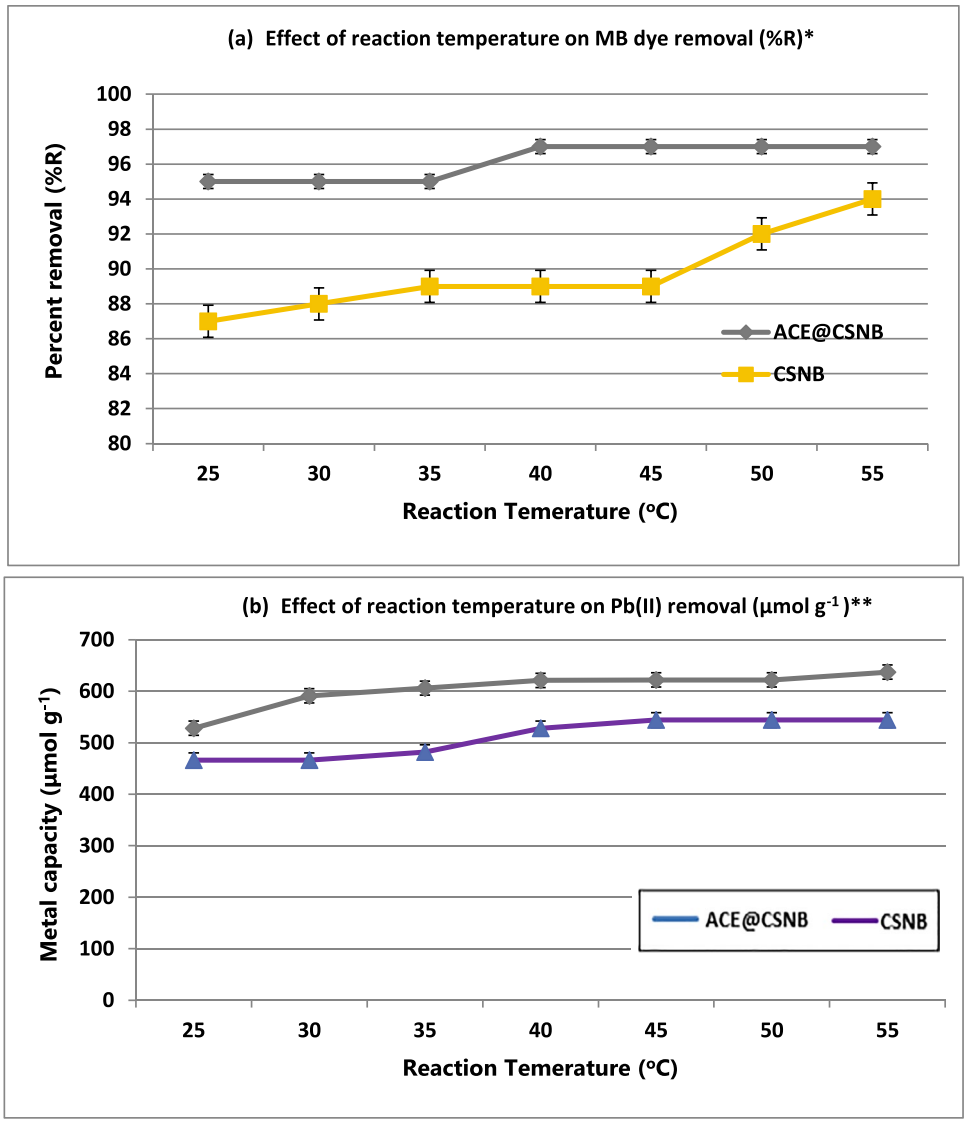

Fig. 5 Comparison of MB dye and Pb(II) removal at different temperatures

the temperature from 25 to 55 °C, respectively. This may be based on the ability of $Pb^{(II)}$ ions to form coordinate bonds with the surface functional groups [61] as illustrated in Scheme 2. The outlined results refer that the binding reactions of $Pb^{(II)}$ ions & MB dye pollutants onto both pristine CSNB and modified ACE@CSNB are mainly correlated to an endothermal behavior. In addition, the superiority trends of the modified ACE@CSNB biochar are also evident when compared to removal efficiency of $Pb^{(II)}$ ions & MB dye pollutants by the pristine CSNB.

3.2.5 The impact and role of pH and point of zero charge

Initially, the points of zero charge (pH_{pzc}) of the modified ACE@CSNB biochar was determined and characterized from the graph of initial pH vs. ΔpH (Fig. 6) to figure out the pH value at which the surface charge is zero. As shown, the pH_{pzc} of ACE@CSNB was identified at 7.0 to refer to the surface neutrality at this point, while at pH < 7.0 and pH > 7.0, the surface of ACE@CSNB biochar turned to be positively and negatively charged, respectively [62]. On the other hand, solution pH is a crucial parameter in the removal process of organic and inorganic pollutants from water and wastewater because this factor is responsible for either protonation or deprotonation of biosorbents as the modified ACE@CSNB and pristine CSNB materials. It is mainly affecting the protonation degree of functional group on the biosorbent surface as well as the selected pollutant species in aqueous solution [63]. The effect of varying the initial pH values of MB solutions (15 mg L^{-1}) and $Pb^{(II)}$ (15 mmo L^{-1}) was investigated and optimized in the range (pH 2.0–10.0) and (pH 2.0–6.0), respectively. This study was performed by using 20 mg of biochar and 30 min of shaking time to evaluate and compare the adsorption capability of the modified

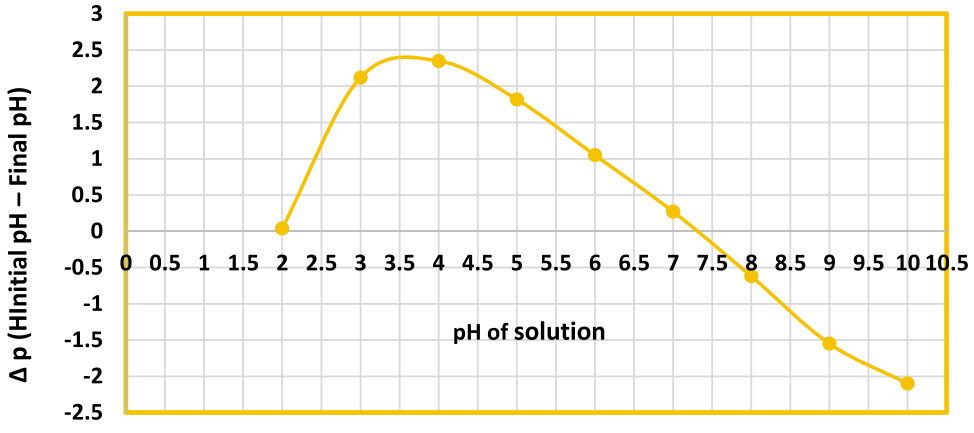

Fig. 6 Point of zero charge (pH_{pzc}) of ACE@CSNB biochar

ACE@CSNB versus pristine CSNB. The figured out values for removal efficiency of MB (R%) and capacity of lead ions (μmol g^{-1}) are illustrated in Fig. 7 a and b, respectively to refer that low removal efficiency (63.5–90.6%) of the modified ACE@CSNB towards MB at pH 1–4. This trend may be attributed to the possible repulsion between positively

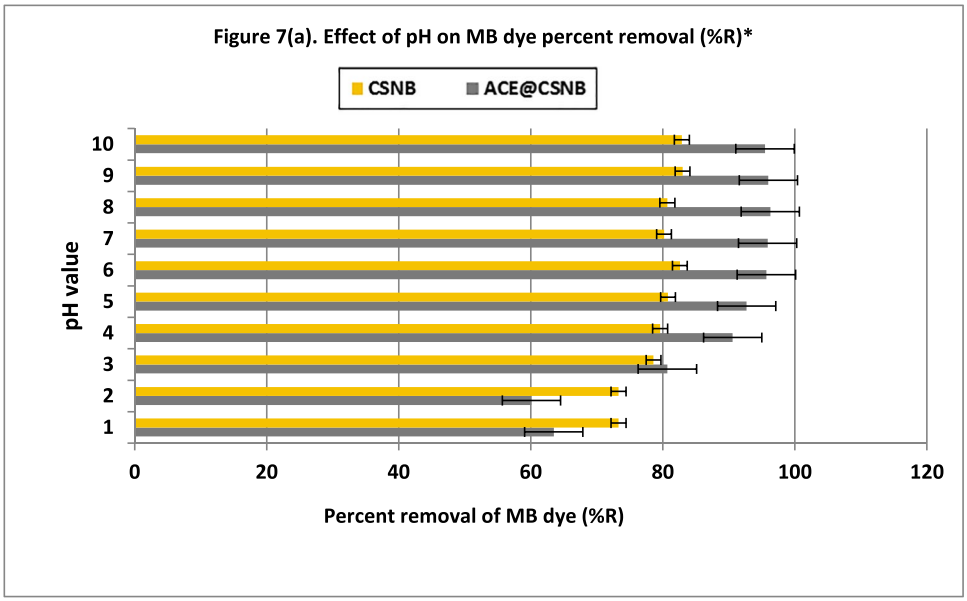

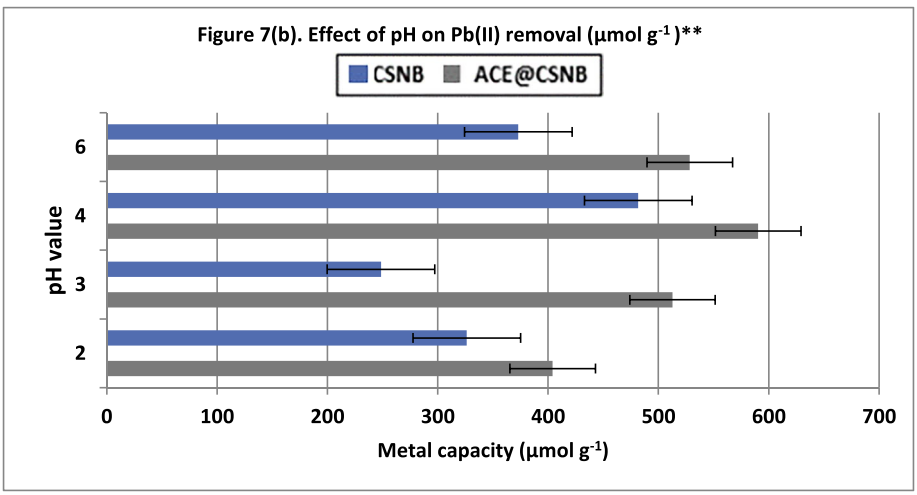

Fig. 7 Comparison of MB dye and Pb(II) removal at different pH conditions

charged surface and positively charged cationic MB. However, by increasing the pH of adsorption reaction, maximum removal value of MB (96.3%) was established by the modified ACE@CSNB to refer to efficient negatively charged surface as deduced from the pH_{pzc} of ACE@CSNB at 7.0 [64]. It is also evident that the lowest percent removal values (%R) of MB were identified at pH 1–3, while the maximum ones were configured at pH 7–10. Moreover, the superior behavior of ACE@CSNB could be characterized when compared versus the pristine CSNB biochar.

The adsorptive removal behaviors of $Pb^{(II)}$ ions onto the modified ACE@CSNB and pristine CSNB were only investigated and compared in the pH 2.0–6.0 to prevent any possible precipitation of lead hydroxide at pH ≥ 7.0 and the collected results are graphed in Fig. 7 b. The same trend was also observed for the increase in the metal capacity (μmol g^{-1}) via raising the pH value of reaction solution from pH 2.0 to 6.0 by both biochar materials with the superiority of ACE@CSNB in comparison to the pristine CSNB biochar.

3.2.6 The impact and role of ionic strength

Due to the negatively charged surface and porosity of modified ACE@CSNB and pristine CSNB materials, other metal cations may be captured via ion pair interaction with the electronegative functional groups and therefore, interfere with the target cationic pollutants having the same charge as $Pb^{(II)}$ & MB pollutants. In addition, the impact of solution ionic strength caused by the presence of Na^+ may highly contribute and interfere in the adsorption of $Pb^{(II)}$ & MB pollutants by ACE@CSNB and CSNB. Thus, it is of practical significance to study the effects of ionic strength by addition of different masses (10–100 mg) of sodium ion to the adsorption reaction. As listed in Table 3, MB removal values onto ACE@CSNB are almost constant and ranged from 88 to 91% to confirm that low (10 mg) or high (100 mg) ionic strength of Na^+ were found to minimally contribute in the adsorptive removal performance of MB. On the other hand, the presence of Na^+ with the pristine CSNB was noticed to increase the percentage removal values of MB from 82% (at 10 mg-NaCl) to 91% high (at 100 mg-NaCl). This may be interpreted by the ability of Na^+ ions to exchange the surface hydrogen ions in the hydroxyl or carboxyl group to enhance good binding with the target MB via cation exchange mechanism [65]. This situation is already existing within the structure ACE@CSNB. However, the trends of adsorptive removal of $Pb^{(II)}$ ions by the modified ACE@CSNB and pristine CSNB materials were characterized to follow the order by increasing the capacity value from 668 to 1678 μmol g^{-1} and from 466 to 606 μmol g^{-1} based on increasing the ionic strength of solution as listed in Table 3. The increase in $Pb^{(II)}$ removal by the modified ACE@CSNB may be attributed to the possible replacement of hydrogen ions by Na^+ in the hydroxyl or carboxyl groups of CSNB component to enhance good binding with the target $Pb^{(II)}$ ions via cation exchange mechanism [66]. Finally, the superior adsorptive behavior of ACE@CSNB versus pristine CSNB is also evident in the study of ionic strength as outlined in Table 3.

3.2.7 Recyclability and reusability of ACE@CSNB

Regeneration of ACE@CSNB nanobiosorbent after its initial application in removal process of $Pb^{(II)}$ ions & MB dye pollutants is very beneficial with respect to the economic feasibility [67]. Recyclability and reusability of ACE@CSNB nanobiosorbent were accomplished by treatment and loaded pollutant desorption from the surface of ACE@CSNB with (50 mL of 0.1 mol L^{-1} HCl). The dry recycled ACE@CSNB nanobiosorbent was then applied in further removal processes of MB dye and $Pb^{(II)}$ pollutants. After the first step of regeneration, the %R of MB was characterized as 92.26% and the q_e value of $Pb^{(II)}$ was identified as 1000 μmol g^{-1}. Moreover, the recycled ACE@CSNB after third recycling procedure was confirmed to remove MB with 75.98% and $Pb^{(II)}$ ions with 633.3 μmol g^{-1} to confirm excellent stability of ACE@CSNB nanobiosorbent for additional recycling and reusability.

Table 3 Comparison of MB dye and Pb(II) removal by CSNB and ACE@CSNB at different ionic strengths of NaCl

Initial concentration	Biochar	Percent removal (%R) ± 1.0%) of MB dye at different ionic strength of added NaCl (mg)*									
		10	**20**	**30**	**40**	**50**	**60**	**70**	**80**	**90**	**100**
15 mg L^{-1} MB dye	**ACE@CSNB**	91	89	89	89	89	89	88	88	89	89
	CSNB	82	84	86	85	86	87	87	87	90	91
Pollutant	**Biochar**	**Metal capacity (μmol g^{-1}) ± 1.0%) of Pb(II) at different ionic strength of added NaCl (mg)****									
		10	**20**	**30**	**40**	**50**	**60**	**70**	**80**	**90**	**100**
15 mmol L^{-1} Pb(II)	**ACE@CSNB**	668	715	730	715	730	746	1150	1305	1461	1678
	CSNB	466	466	513	513	513	529	482	513	544	606

*%R values are the average of triplicate run with ± **1.0%**

μmol g^{-1} capacity values are the average of triplicate run with ± **0.4%

3.2.8 *Remediation of $Pb^{(II)}$ & MB pollutants from various water matrices*

The potential practical application of the modified ACE@CSNB in efficient removal of $Pb^{(II)}$ & MB pollutants from various samples is an important final evaluation step. This study was accomplished by the batch equilibrium technique to ensure efficient competence for removal of these two cationic pollutants from different water sources. The selected samples include wastewater, sea water and tap water were spiked to produce 10 and 15 mg L^{-1} of both $Pb^{(II)}$ & MB pollutants. The selected and examined water samples (100 mL) were then mixed with 50 mg of ACE@CSNB and automatically shaken. The removal (%) of $Pb^{(II)}$ & MB pollutants were calculated as listed in Table 4. It is evident that the removal efficiency values of MB from the three water matrices were characterized as 93.37–98.19% (10 mg L^{-1}) and 91.74–98.02% (15 mg L^{-1}) and those related to $Pb^{(II)}$ ions were in the range 96.27–98.50% (10 mg L^{-1}) and 99.00–99.14% (15 mg L^{-1}). The collected results from this study confirm the validity and applicability of the investigated ACE@CSNB biochar for treatment of $Pb^{(II)}$ ions & MB dye pollutants from real effluents with excellent removal performance.

4 Conclusion

A successful hydrothermal and solvothermal microwave irradiation process was used to prepare a modified ACE@CSNB biochar in only few minutes. The as-prepared ACE@CSNB was characterized and proved to exhibit higher total pore volume and mean pore size compared to the pristine CSNB biochar. The assembled ACE@CSNB biochar was found more homogenous due to surface loading of the sulfonate group as characterized by the FT-IR stretching bands at 1140–1250 cm^{-1} and 1030–1070 cm^{-1} for R-SO_3^- with S = O. The adsorption behavior of ACE@CSNB was compared versus the pristine CSNB in removal of $Pb^{(II)}$ & MB dye pollutants. The evaluated and optimized parameters revealed and referred to high adsorption performance of $Pb^{(II)}$ ions & MB dye by ACE@CSNB when compared with the pristine CSNB under the impact of biochar dose, reaction time, initial pollutant concentration, reaction temperature, pH and ionic strength of contact solution. In addition, ACE@CSNB was found highly stable to regeneration and reapplication with respect to removal of MB and $Pb^{(II)}$ providing 92.26% and 1000 μmol g^{-1}, respectively. The removal efficiency and capability of ACE@CSNB biochar were also confirmed via recovery of MB from the three real tap, sea and industrial wastewater matrices providing 93.37–98.19% (10 mg L^{-1}) and 91.74–98.02% (15 mg L^{-1}) and those related recovery percentage values to $Pb^{(II)}$ ions were 96.27–98.50% (10 mg L^{-1}) and 99.00–99.14% (15 mg L^{-1}). This study confirmed the validity and applicability of ACE@CSNB biochar in remediation of the two investigated cationic $Pb^{(II)}$ ions & MB dye pollutants from real effluents with excellent removal performance. Moreover, the sustainability and low-cost aspects of ACE@CSNB biochar afford other significant dimensions in water treatment and purification from miscellaneous cationic pollutants.

5 Disclaimer

1. The authors of this manuscript agree to submit this manuscript for publication in ***Biomass Conversion and Biorefinery***.
2. The authors of this manuscript wish to confirm that there are no known conflicts of interest associated with this publication and there has been no significant financial support for this work that could have influenced its outcome.
3. The authors confirm that the manuscript has been read and approved by all authors and that there are no other persons who satisfied the criteria for authorship but are not listed. We further confirm that the order of authors listed in the manuscript has been approved by all of us.
4. The authors understand that the Corresponding Author is the sole contact for the Editorial process including the editorial manager. He is responsible for communicating with the other authors about progress, submissions of revisions and final approval of proofs.

Supplementary Information The online version contains supplementary material available at https://doi.org/10.1007/s13399-023-04098-9.

Table 4 Application of **ACE@CSNB** in removal MB dye and Pb(II) pollutants from various water matrices*

Spiked concentration	Percent removal (R%) of MB dye from water matrices			Percent removal (R%) of Pb(II) from water matrices		
	Sea water	Wastewater	Tap water	Sea water	Wastewater	Tap water
10 mg L^{-1}	93.37	98.80	98.19	98.50	96.27	96.71
15 mg L^{-1}	91.74	93.18	98.02	99.04	99.00	99.14

*%R values are the average of triplicate run with ± **1.3%**

Acknowledgements The authors of this manuscript acknowledge the technical supports provided by Arab Academy for Science and Technology and Maritime Transport, Alexandria, Egypt—University of Oviedo, Oviedo, Spain—Alexandria University, Alexandria, Egypt.

Author contribution Safe ELdeen M.E. Mahmoud: experimental, data collection, characterization, writing and editing. David Ursueguia: characterization. Mohamed E. Mahmoud: supervision, conceptualization, writing- reviewing and editing. Tarek Abdel-Fattah: supervision, conceptualization, writing- reviewing and editing. Eva Diaz: supervision, conceptualization, writing- reviewing and editing.

Funding Open access funding provided by The Science, Technology & Innovation Funding Authority (STDF) in cooperation with The Egyptian Knowledge Bank (EKB). After acceptance of this submission, it will be funded to publish as "Open Access" by The Science, Technology & Innovation Funding Authority (STDF) in cooperation with The Egyptian Knowledge Bank (EKB).

Data availability Data will be available upon request from the corresponding author (Mohamed E. Mahmoud).

Declarations

Ethical approval Not applicable.

Competing interests The authors declare no competing interests.

References

1. Zeghioud H, Fryda L, Djelal H, Assadi A, Kane A (2022) A comprehensive review of biochar in removal of organic pollutants from wastewater: characterization, toxicity, activation/functionalization and influencing treatment factors. J Water Proc Eng 47:102801
2. Jeyasubramanian K, Thangagiri B, Sakthivel A, Raja JD, Seenivasan S, Vallinayagam P, Madhavan D, Devi SM, Rathika B (2021) A complete review on biochar: production, property, multifaceted applications, interaction mechanism and computational approach. Fuel 292:120243
3. Luo K, Pang Y, Wang D, Li X, Wang L, Lei M, Huang Q, Yang Q (2021) A critical review on the application of biochar in environmental pollution remediation: role of persistent free radicals (PFRs). J Environ Sci (China) 108:201–216
4. Nithyalakshmi B, Saraswathi R (2021) Removal of colorants from wastewater using biochar derived from leaf waste. Biomass Conv Bioref. https://doi.org/10.1007/s13399-021-01776-4
5. Guo J, Xiao H, Zhang JB (2022) Characterization of highly stable biochar and its application for removal of phenol. Biomass Conv Bioref. https://doi.org/10.1007/s13399-022-03375-3
6. Bentahar Y. Lomenech C, Mija A (2022) Adsorptive properties of biochar derived from biorefinery industry for basic dye removal. Biomass Conv Bioref. https://doi.org/10.1007/s13399-022-03398-w
7. Thillainayagam BP, Nagalingam R, Saravanan P (2022) Batch and column studies on removal of methylene blue dye by microalgae biochar. Biomass Conv Bioref. https://doi.org/10.1007/s13399-022-03038-3
8. Mahmoud ME, El-Ghanam, AM, Saad SR (2022) Sequential removal of chromium (VI) and prednisolone by nanobiochar-enriched-diamine derivative. Biomass Conv SBioref. https://doi.org/10.1007/s13399-022-02888-1
9. Mahmoud ME, Abou-Ali SAAE, Elweshahy SMT (2021) Efficient and ultrafast removal of Cd(II) and Sm(III) from water by leaves of Cynara scolymus derived biochar. Mater Res Bull 141:111334
10. Liu S, Li J, Xu S, Wang M, Zhang Y, Xue X (2019) A modified method for enhancing, adsorption capability of banana pseudostem biochar towards methylene blue at low temperature. Bioresour Technol 282:48–55
11. Cao Y, Shen G, ZhangY GC, Li Y, Zhang P, Xiao W, Han L (2019) Impacts of carbonization temperature on the Pb (II) adsorption by wheat straw-derived biochar and related mechanism. Sci Total Environ 692:479–489
12. Kim JE, Bhatia SK, Song HJ, Yoo E, Jeon HJ, Yoon JY, Yang Y, Gurav R, Yang YH, Kim HJ, Choi YK (2020) Adsorptive removal of tetracycline from aqueous solution by maple leaf-derived biochar. Bioresour Technol 306:123092
13. Patel M, Kumar R, Pittman CU, Mohan D (2021) Ciprofloxacin and acetaminophen, sorption onto banana peel biochars: environmental and process parameter, influences. Environ Res 201:111218
14. Shakya A, Agarwal T (2019) Removal of Cr(VI) from water using pineapple peel derived biochars: adsorption potential and re-usability assessment. J Mol Liq 293:111497
15. Wang P, Liu X, Yu B, Wu X, Xu J, Dong F, Zheng Y (2020) Characterization of peanut shell biochar and the mechanisms underlying its sorption for atrazine and nicosulfuron in aqueous solution. Sci Total Environ 702:134767
16. Liang L, Xi F, Tan W, Meng X, Hu B, Wang X (2021) Review of organic and inorganic pollutants removal by biochar and biochar-based composites. Biochar 3:255–281
17. Wang S, Bian S, Liu J, Li J, Xu S, Liang Z (2021) Highly adsorptive pristine and magnetic biochars prepared from crayfish shell for removal of Cu(II) and Pb(II). J Taiwan Inst Chem Eng 127:175–185
18. Rangabhashiyam S, Balasubramanian P (2019) The potential of lignocellulosic biomass precursors for biochar production: Performance, mechanism and wastewater applicationa review. Ind Crops Prod 128:405–423
19. Dawood S, Sen TK, Phan C (2017) Synthesis and characterization of slow pyrolysis pine cone bio-char in the removal of organic and inorganic pollutants from aqueous solution by adsorption: kinetic, equilibrium, mechanism and thermodynamic. Bioresource Technol 246:76–81
20. Mahmoud ME, El-Bahy SM, Elweshahy SMT (2021) Decorated Mn-ferrite nanoparticle@Zn–Al layered double hydroxide@ Cellulose@ activated biochar nanocomposite for efficient remediation of methylene blue and mercury (II). Bioresour Technol 342:126029
21. Gokulan R, Ganesh Prabhu G, Jegan J (2019) A novel sorbent Ulva lactuca-derived biochar for remediation Remazol brilliant orange 3R in packed column. Water Environ Res 91:642–649
22. Mahmoud ME, Abouelanwar ME, Mahmoud SME, El-Bahy SM (2021) Novel immobilized fibrous natural cotton on Corchorus olitorius stalks biochar@ diethylenetriamine@ feroxyhyte@

diethylenetriamine composite for coagulative removal of silver quantum dots (Ag-QDs) from water. Cellulose 28:11397–11416
23. Jin J, Kang M, Sun K, Pan Z, Wu F, Xing B (2016) Properties of biochar-amended soils and their sorption of imidacloprid, isoproturon, and atrazine. Sci Total Environ 550:504–513
24. Kumar M, Gokulan R, Sujatha S et al (2021) Biodecolorization of reactive red 120 in batch and packed bed column using biochar derived from Ulva reticulata. Biomass Convers Biorefinery. https://doi.org/10.1007/s13399-020-01268-x
25. Nguyen DLT, Binh QA, Nguyen XC, Nguyen TTH, Vo QN, Nguyen TD, Tran TCP, Nguyen TAH, Kim SY, Nguyen TP, Bae J, Kim IT, Van Le Q (2021) Metal salt-modified biochars derived from agro-waste for effective Congo red dye removal. Environ Res 200:111492
26. Hu B, Tang Y, Wang X, Wu L, Nong J, Yang X, Guo J (2021) Cobalt-gadolinium modified biochar as an adsorbent for antibiotics in single and binary systems. Microchem J 166:106235
27. Abdoul Magid ASI, Islam MS, Chen Y, Weng L, Li J, Ma J, Li Y (2021) Enhanced adsorption of polystyrene nanoplastics (PSNPs) onto oxidized corncob biochar with high pyrolysis temperature. Sci Total Environ 784:147115
28. Navarathna CM, Dewage NB, Keeton C, Pennisson J, Henderson R, Lashley B, Zhang X, Hassan E, Perez F, Mohan D, Pittman CU Jr, Mlsna T (2020) Biochar Adsorbents with Enhanced Hydrophobicity for Oil Spill Removal. ACS Appl Mater Interfaces 12:9248–9260
29. Fang L, Miao Y, Wei D, Zhang Y, Zhou Y (2021) Efficient removal of norfloxacin in water using magnetic molecularly imprinted polymer. Chemosphere 262:128032
30. Kasak K, Truu J, Ostonen I, Sarjas J, Oopkaup K, Paiste P, Truu M (2018) Biochar enhances plant growth and nutrient removal in horizontal subsurface flow constructed wetlands. Sci Total Environ 639:67–74
31. Geng X, Lv S, Yang J, Cui S, Zhao Z (2021) Carboxyl-functionalized biochar derived from walnut shells with enhanced aqueous adsorption of sulfonamide antibiotics. J Environ Manag 280:111749
32. Schwantes D, Jr ACG, Campagnolo MA, Tarley CRT, Dragunski DC, de Varennes A, Silva AKS, Junior EC (2018) Chemical modifications on pinus bark for adsorption of toxic metals. J Environ Chem Eng 6:1271–1278
33. Hu Y, Zhu Y, Zhang Y, Lin T, Zeng G, Zhang S, Wang Y, He W, Zhang M, Long H (2019) An efficient adsorbent: simultaneous activated and magnetic ZnO doped biochar derived from camphor leaves for ciprofloxacin adsorption. Bioresour Technol 288:121511
34. Iqbal J, Noor S, Shah B, Sayed CM, Niazi NK, Imran M, Khan JA, Khan ZUH, Hussien AGS, Polychronopoulou K, Howari F (2021) Nano-zerovalent manganese/biochar composite for the adsorptive and oxidative removal of Congo-red dye from aqueous solutions. J Hazard Mater 403:123854
35. Inam E, Udo O, Edet J, Etim U, Offiong N (2018) Adsorption of methylene blue from aqueous solution by humic acid extracted from freshwater river humus. J Mater Environ Sci 9:1324–1334
36. Kanwal A, Farhan M, Sharif F, Hayyat MU, Shahzad L, Ghafoor GZ (2020) Effect of industrial wastewater on wheat germination, growth, yield, nutrients and bioaccumulation of lead. Sci Rep 10:1–9
37. Hosseini H, Zirakjou A, McClements DJ, Goodarzi V, Chen W-H (2022) Removal of methylene blue from wastewater using ternary nanocomposite aerogel systems Carboxymethyl cellulose grafted by polyacrylic acid and decorated with graphene oxide. J Hazard Mater 421:126752
38. Mahmood T, Saddique MT, Naeem A, Westerhoff P, Mustafa S, Alum A (2011) Comparison of different methods for the point of zero charge determination of NiO. Ind Eng Chem Res 50:17
39. Kabiri K, Zohuriaan-Mehr MJ, Mirzadeh H, Kheirabadi M (2010) Solvent-, ion- and pH-specific swelling of poly(2-acrylamido-2-methylpropane sulfonic acid) superabsorbing gels. J Polym Res 17:203–212
40. Li M, Liu H, Chen T, Dong C, Sun Y (2019) Synthesis of magnetic biochar composites for enhanced uranium (VI) adsorption. Sci Total Environ 651:1020–1028
41. Cai W, Wei J, Li Z, Liu Y, Zhou J, Han B (2019) Preparation of amino-functionalized magnetic biochar with excellent adsorption performance for Cr(VI) by a mild one-step hydrothermal method from peanut hull. Colloids and Surf A 563:102–111
42. Guo C, Zou J, Yang J, Wang K, Song S (2020) Surface characterization of maize-strawderived biochar and their sorption mechanism for Pb^{2+} and methylene blue. PLoS ONE 15:e0238105
43. Patino Y, Diaz E, Ordonez S, Gallegos-Suarez E, Guerrero-Ruiz A, Rodriguez-Ramos I (2015) Adsorption of emerging pollutants on functionalized multiwall carbon Nanotubes. Chemosphere 136:174–180
44. Cuervo MR, Asedegbega-Nieto E, Dıaz E, Ordonez S, Vegaa A, Dongil AB, Rodrıguez-Ramos I (2008) Modification of the adsorption properties of high surface area graphites by oxygen functional groups. Carbon 46:2096–2106
45. Li X, Shen Q, Zhang D, Mei X, Ran W, Xu Y, Yu G (2013) Functional groups determine biochar properties (pH and EC) as studied by two-dimensional 13C NMR correlation spectroscopy. PLoS ONE 8:e65949
46. Liebau F (2003) Ordered microporous and mesoporous materials with inorganic hosts: definitions of terms, formula notation, and systematic classification. Micropor Mesopor Mat 58:15–72
47. Biswal BK, Vijayaraghavan K, Tsen-Tieng DL, Balasubramanian R (2022) Biochar-based bioretention systems for removal of chemical and microbial pollutants from stormwater: A critical review. J Hazard Mater 422:126886
48. Karimi S, Tavakkoli Yaraki M, Karri RR (2019) A comprehensive review of the adsorption mechanisms and factors influencing the adsorption process from the perspective of bioethanol dehydration. Renew Sustain Energy Rev 107:535–553
49. Wen Z, Xi J, Lu J, Zhang Y, Cheng G, Zhang Y, Chen R (2021) Porous biochar-supported $MnFe_2O_4$ magnetic nanocomposite as an excellent adsorbent for simultaneous and effective removal of organic/inorganic arsenic from water. J Hazard Mater 411:124909
50. Zhang Y, Fan R, Zhang Q, Chen Y, Sharifi O, Leszczynska D, Zhang R, Dai Q (2019) Synthesis of $CaWO_4$-biochar nanocomposites for organic dye removal. Mater Res Bull 110:169–173
51. Park JH, Wang JJ, Meng Y, Wei Z, DeLaune RD, Seo DC (2019) Adsorption/desorption behavior of cationic and anionic dyes by biochars prepared at normal and high pyrolysis temperatures. Colloids Surf A 572:274–282
52. Gokulan R, Avinash A, Prabhu GG, Jegan J (2019) Remediation of remazol dyes by biochar derived from Caulerpa scalpelliformis—an eco-friendly approach. J Environ Chem Eng 7:103297
53. Son E, Poo K, Chang J, Chae K (2018) Heavy metal removal from aqueous solutions using engineered magnetic biochars derived from waste marine macro-algal biomass. Sci Total Environ 615:161–168
54. Holliday MC, Parsons DR, Zein SH (2022) Agricultural pea waste as a low-cost pollutant biosorbent for methylene blue removal: adsorption kinetics, isotherm and thermodynamic studies, Biomass Conver Bioref. https://doi.org/10.1007/s13399-022-02865-8
55. Nouacer I, Benalia M, Henini G, Djedid M, Laidani Y (2022) Mathematical modeling and interpretation of equilibrium isotherms of Pb(II) from aqueous media by Chlorella pyrenoidosa immobilized in Luffa cylindrica. Biomass Conv Bioref. https://doi.org/10.1007/s13399-021-01722-4

56. Sewu DD, Woo SH, Lee DS (2021) Biochar from the co-pyrolysis of Saccharina japonica and goethite as an adsorbent for basic blue 41 removal from aqueous solution. Sci Total Environ 797:149160
57. Zheng Y, Wang J, Li D, Liu C, Lu Y, Lin X, Zheng Z (2021) Insight into the KOH/KMnO4 activation mechanism of oxygen-enriched hierarchical porous biochar derived from biomass waste by in-situ pyrolysis for methylene blue enhanced adsorption. J Anal Appl Pyrolysis 158:105269
58. Emrooz HBM, Maleki M, Rashidi A, Shokouhimehr M (2021) Adsorption mechanism of a cationic dye on a biomass-derived microand mesoporous carbon: structural, kinetic, and equilibrium insight, Biomass Conver. Bioref 11:943–954
59. Chand P, Pakad, Y (2022) Decontamination of toxic Pb^{+2}, Cd^{+2}, and Ni^{+2} from the liquid medium using modified apple juice industrial biomass: isotherm and kinetic study. Biomass Conv Bioref. https://doi.org/10.1007/s13399-022-03339-7
60. Mu Y, Ma H (2021) NaOH-modified mesoporous biochar derived from tea residue for methylene Blue and Orange II removal. Chem Eng Res Des 167:129–140
61. Lu H, Zhang W, Yang Y, Huang X, Wang S, Qiu R (2012) Relative distribution of Pb^{2+} sorption mechanisms by sludge-derived biochar. Water Res 46:854–862
62. Wang Y, Jiang B, Wang L, Feng Z, Fan H, Sun T (2021) Hierarchically structured two-dimensional magnetic microporous biochar derived from hazelnut shell toward effective removal of p-arsanilic acid. Appl Surf Sci 540:148372
63. Yu KL, Lee XJ, Ong HC, Chen WH, Chang JS, Lin CS, Show PL, Ling TC (2021) Adsorptive removal of cationic methylene blue and anionic Congo red dyes using wet-torrefied microalgal biochar: equilibrium, kinetic and mechanism modeling. Environ Pollut 272:115986
64. Mahmood T, Saddique MT, Naeem A, Westerhoff P, Mustafa S, Alum A (2011) Comparison of different methods for the point of zero charge determination of NiO. Ind Eng Chem Res 50:10017–10023
65. Saha P, Chowdhury S, Gupta S, Kumar I (2010) Insight into adsorption equilibrium, kinetics and thermodynamics of Malachite Green onto clayey soil of Indian origin. Chem Eng J 165:874–882
66. Lalmi A, Bouhidel K, Sahraoui B, Anfif C (2018) Removal of lead from polluted waters using ion exchange resin with Ca(NO3)2 for elution. Hydrometallurgy 178:287–293
67. Nguyen LHT, Nguyen HTT, Le BQG, Dang MD, Nguyen TTT, Mai NXD, Doan TLH (2022) Microwave-assisted solvothermal synthesis of defective zirconium-organic framework as a recyclable nano-adsorbent with superior adsorption capacity for efficient removal of toxic organic dyes. Colloid Interf Sci Commun 46:100511